Geoscience Frontiers 14 (2023) 101525

Contents lists available at ScienceDirect

Geoscience Frontiers

journal homepage: www.elsevier.com/locate/gsf

Research Paper

Nature and evolution of the lower crust under central Spain: Inferences from granulite xenoliths (Calatrava Volcanic Field-Spanish central system)

David Orejana [a,*], Carlos Villaseca [a,b], Marlina A. Elburg [c], Enrique Merino-Martínez [d], Javier García Serrano [a]

[a] Departamento de Mineralogía y Petrología, Universidad Complutense de Madrid, Spain
[b] Departamento de Dinámica Terrestre y Observación de la Tierra, Instituto de Geociencias IGEO (UCM, CSIC), Madrid, Spain
[c] Department of Geology, University of Johannesburg, South Africa
[d] Instituto Geológico y Minero de España – Consejo Superior de Investigaciones Científicas, CN IGME – CSIC

ARTICLE INFO

Article history:
Received 15 August 2022
Revised 11 November 2022
Accepted 4 December 2022
Available online 9 December 2022
Handling Editor: K. Szilas

Keywords:
Granulite xenoliths
U–Pb geochronology
Lu–Hf isotopes
Calatrava Volcanic Field
Spanish central system

ABSTRACT

So far, the nature and evolution of the lower crust under central Spain have been constrained mainly on the basis of a heterogeneous suite of granulite xenoliths from the Spanish Central System (SCS). In recent years, ultramafic volcanics from the Calatrava Volcanic Field (CVF) have also provided deep-seated crustal xenoliths which have not been studied in detail. Our data, combining mineral, whole-rock and isotopic geochemistry with U–Pb–Hf isotope ratios in zircons from the CVF and SCS xenoliths, highlight the felsic composition of the lower crust under central Iberia. A number of the Calatrava xenoliths represents Variscan igneous protoliths, which are a minor population in the SCS, and were likely formed by crystallisation of intermediate and felsic melts in the lower crust during the Variscan orogeny (leucodiorite protolith age of 314 ± 3 Ma and leucogranite protolith age of 308 ± 2.5 Ma). U–Pb data of metamorphic zircons show that granulite-facies metamorphism mainly occurred from 299 to 285 Ma in both areas. These ages are slightly younger than those of granitic intrusions that could be genetically related to the granulitic residue, which points to a main role of U–Pb isotope resetting in lower crustal zircons during HT or UHT conditions. The zircon U–Pb–Hf isotopic ratios support the idea that the lower crust in central Iberia consists mainly of Ordovician–Neoproterozoic metaigneous and metasedimentary rocks associated with the Cadomian continental arc of northern Gondwana. These rocks provide evidence of mixing between juvenile magmas and an enriched crustal component, ultimately extracted from an Eburnean crust. Other more evolved components present in detrital zircons are likely related to recycling of Archean crust derived from North Africa cratonic terranes.

1. Introduction

The composition of the deep continental crust is difficult to establish as it is usually inaccessible. Its study is mainly based on tectonically exhumed granulite terranes of orogenic settings and deep-seated granulite xenoliths entrapped into mafic volcanic and subvolcanic magmas. After many years of research, it has become clear that the lower crust is highly heterogeneous and usually more mafic than the middle and upper crust (e.g., Rudnick and Gao, 2003). Nevertheless, in some regions, the lower crust is relatively felsic, displaying a composition similar to andesites and dacites (Hacker et al., 2015). Some of these felsic sections have been described for the French Massif Central (e.g., Downes et al., 1990) and central Spain (Villaseca et al., 1999), where granulite xenoliths with an intermediate to felsic composition represent more than half the xenolith population. Lower crustal felsic rocks may be of igneous or sedimentary derivation and contain information related to old magmatic and metamorphic events essential for understanding the lithospheric evolution and crustal growth mechanisms.

In central Spain, the abundant felsic granulite xenoliths from the Spanish Central System (SCS) are interpreted as Neoproterozoic and Early Paleozoic igneous and sedimentary rocks that were reworked during the Variscan continental collision (Villaseca et al., 1999, 2011; Orejana et al., 2011). The presence of minor proportions of mafic rocks in this lower crustal section has been

* Corresponding author at: Department of Mineralogy and Petrology, Complutense University of Madrid, Calle José Antonio Novais 12, 28040 Madrid, Spain.
E-mail address: dorejana@ucm.es (D. Orejana).

https://doi.org/10.1016/j.gsf.2022.101525
1674-9871/

related to underplating of mafic magmas of unconstrained age (Orejana et al., 2006; Villaseca et al., 2007b). Moreover, the U–Pb–Hf isotope composition of zircons from these felsic granulites supports the contribution of a pre-Neoproterozoic crustal component, although the age and origin of such a component are still unclear (Orejana et al., 2011; Villaseca et al., 2011). Recently, a new outcrop with lower crustal granulite xenoliths has been described in the Calatrava Volcanic Field (CVF), located to the south of the SCS (Puelles et al., 2019) (Fig. 1). Although of felsic composition, these xenoliths display some differences with respect to the SCS granulites, such as the higher proportion of intermediate lithologies (leuco *meta*-norites and *meta*-anorthosites) and their Variscan age (309 ± 3 Ma; Puelles et al., 2019). However, the lack of a detailed whole-rock (major, trace elements and Sr–Nd isotopes) and zircon (trace elements and Hf isotopes) geochemical characterization, combined with insufficient U–Pb geochronological data on some of these CVF xenoliths, leaves many issues unconstrained, including the metaigneous or metasedimentary origin of these granulites.

Thus, in the present work we have collected a new set of granulite xenoliths from the La Encomienda volcano (CVF) and also a selection of felsic xenoliths from the SCS, including metasedimentary types that have not been studied previously for U–Pb zircon dating (Table 1). A complete data set of the former xenoliths is provided, including major and trace element mineral chemistry, whole-rock major and trace element contents, Sr–Nd isotopic signatures and zircon U–Pb–Hf isotopes. The selected SCS samples were previously studied with respect to petrography, mineral chemistry and whole-rock geochemistry (Villaseca et al., 1999), but here we present a large data set regarding the trace element and U–Pb–Hf isotopic composition of zircon. These data from CVF and SCS granulite xenoliths have allowed a detailed characterization of their whole-rock composition, the estimation of the *P-T* conditions of metamorphic equilibrium and the discussion of age differences between granulitization and protolith formation. Moreover, the dating of magmatic and sedimentary protoliths allows for constraining the nature and evolution of the lower crust under central Spain, highlighting the differences between the two sampling areas.

2. Geological setting

The Central Iberian Zone (CIZ) is the innermost region within the Variscan Belt exposed in the Iberian Massif. It is mainly composed of Neoproterozoic to Early Paleozoic metasedimentary rocks and Cambrian–Ordovician metaigneous rocks, with all these units intruded by abundant late- to post-tectonic felsic intrusions (granitoids) during the Variscan orogeny (Fig. 1). The granulite xenoliths studied in this work are lower crustal material entrained by mafic alkaline post-Variscan subvolcanic rocks from the Spanish Central System (SCS) and also by the olivine melilitite of the La Enco-

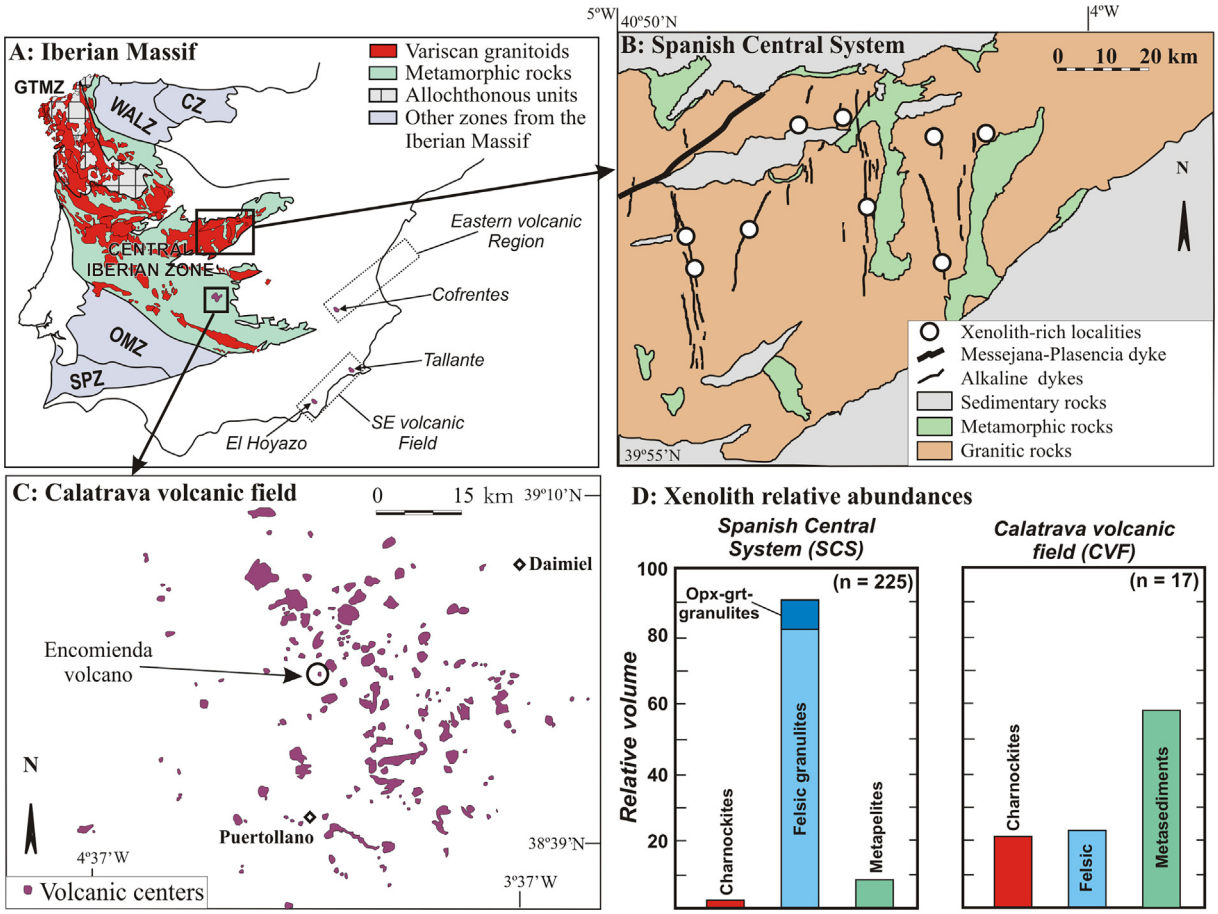

Fig. 1. Schematic representation of the Iberian Massif (A) indicating the areas where lower crustal granulite xenoliths have been found in the Central Iberian Zone: the Spanish Central System (SCS) (B) and the Calatrava Volcanic Field (CVF) (C). White circles in (B) indicate the outcrops with xenoliths. Location of xenolith-bearing volcanoes from Iberian eastern and southeastern Cenozoic volcanic regions are also shown (Cofrentes, Tallante and El Hoyazo). CZ: Cantabrian Zone; GTMZ: Galicia-Tras-Os-Montes Zone; WALZ: West Asturian-Leonese Zone; OMZ: Ossa Morena Zone; SPZ: South Portuguese Zone. (D) Relative abundance of the different xenolith types from the SCS and the CVF sectors based on number of samples from each group and averaged xenolith size (SCS data slightly modified from Villaseca et al., 2007b).

Table 1
Main features of the studied Calatrava and SCS granulite xenoliths.

Sample	Type	Modal mineral composition (vol.%)	Nature of granulite	Granulite-facies age (Ma)*	Variscan igneous cores (% and age)	Pre-Variscan inheritances (%)
Calatrava Volcanic Field						
117449	I: charnockite	Main: pl (67), opx (25), grt (7). Accessories (1) : rt, qtz, ap, mag, zrn, mnz.	Leucodioritic cumulate	299 (+5.6/−3.6)	87.8 314 (+4.1/−1.9) Ma	2.2
117451	I: charnockite	Main: pl (70), opx (21), bt (8). Accessories (1) : rt, ap, mag, zrn, mnz.	Leuconoritic cumulate		–	–
117453	II: garnet felsic	Main: pl (45), qtz (28), kfs (14), grt (10). Accessories (3): bt (2) , rt, ap, ilm, zrn.	Residual metasediment		–	–
117454	II: garnet felsic	Main: kfs (40), pl (30), qtz (20), grt (8). Accessories (2): bt (1) , rt, ap, ilm, zrn.	Residual metasediment		–	–
117455	II: garnet felsic	Main: kfs (30), pl (27), qtz (20), grt (20). Accessories (3) : phl, rt, sil, ap, mag, zrn.	Residual metasediment	282–293? Ma	0	84.2
117448	III: metagranite	Main: kfs (50), qtz (25), pl (24). Accessories (1) : ap, zrn, op.	Granitic intrusive		–	–
117450	III: metagranite	Main: pl (40), kfs (32), qtz (20), bt (7). Accessories (1) : ap, zrn, op.	Granitic intrusive	292 ± 3.8	51.2 308 (+3.2/−0.4) Ma	18.8
117452	III: metatonalite	Main: pl (74), qtz (15), kfs (5), bt (5). Accessories (1) : ap, zrn, op.	Tonalitic intrusive		–	–
Spanish Central System						
77746	Metapelitic	Main: kfs (39), grt (26), qtz (15), pl (10), sil (8). Accessories (2) : rt, ap, zrn, mnz.	Residual metapelite	277 ± 1.9	0	0**
77750	Metapelitic	Main: kfs (45), grt (22), qtz (18), sil (13). Accessories (2) : rt, ap, zrn, mnz.	Residual metapelite	289 ± 4.0	0	51.6
U50	Felsic metaigneous	Main: grt (41), kfs (33), pl (20), qtz (3). Accessories (3) : phl, rt, ap, zrn.	Residual metaigneous rock	288 ± 3.5	0	17.2
99187	Felsic metaigneous	Main: kfs (38), grt (25), pl (20), qtz (15). Accessories (2) : rt, ap, zrn.	Residual metaigneous rock	285 ± 2.8	0	44.8

*The age data are Tuffzirc or weighted average ages (excepting sample 117455) from this study. The range of ages given for sample 117455 represent the youngest ages obtained in 3 zircon rims (see text for more detail). **See explanation in section 7 of the text.

mienda volcano from the Calatrava Volcanic Field (CVF), located in central–southern CIZ.

The SCS is a mountain range where rocks of the CIZ are exposed: mainly granitic intrusions (309–298 Ma; Orejana et al., 2012 and references therein) emplaced within metasediments and orthogneisses. This granitic batholith is crosscut by post-Variscan upper Permian alkaline ultramafic lamprophyre and diabase dykes (Fig. 1A) which carry a heterogeneous xenolith population, including deep-seated granulitic and pyroxenitic varieties (Villaseca et al., 1999, 2007b; Orejana et al., 2006; Orejana and Villaseca, 2008). The mineral and whole-rock composition of the SCS granulitic xenoliths have been studied in detail (Villaseca et al., 1999, 2007b), and they have been classified as charnockitic, metapelitic and metaigneous felsic granulites, the latter being the most abundant group (up to 93 vol.%; Villaseca et al., 2007b). Pressure and temperature estimates, either using classic geothermobarometers or modern methods based on the Ti and Zr contents in zircon and rutile, respectively, indicate a lower crustal provenance (~0.8–1.2 GPa; Villaseca et al., 1999) and high-grade metamorphism (~850–1000 °C; Villaseca et al., 1999; Orejana et al., 2011). The presence of kelyphitic coronas around granulitic garnets implies a high-*T* low-*P* paragenesis and re-equilibration during transport in the alkaline magma. It has been suggested that these granulite xenoliths might represent the residue left after the extraction of the felsic melts that formed the granitic SCS batholith (e.g., Villaseca et al., 1999). Two U–Pb geochronological studies (Fernández-Suárez et al., 2006; Orejana et al., 2011) on three SCS felsic granulite xenoliths have revealed an abundant Variscan age population (peaks at ~283–298 Ma) and several groups of inherited ages (Cambrian–Ordovician, Ediacaran–Cryogenian and scarce older ages). These data, together with the zircon Hf isotopic signatures, point to the contribution of two distinct components to the origin of the igneous protolith: relatively juvenile Cadomian magmas and an unconstrained recycled older crust (Villaseca et al., 2011).

The CVF comprises about 250 monogenetic volcanic centres (scoria cones and maars; Fig. 1B) formed mainly by the eruption of Pliocene–Pleistocene olivine-bearing alkaline basalts, basanites, nephelinites and melilitites (Ancochea, 1982), which crop out within an Ordovician–Silurian basement of low-grade metamor-

phic rocks partially overlain by Miocene to Quaternary fluvial and lacustrine sediments. Several CVF volcanoes present lava flows or pyroclastic deposits showing a varied suite of deep-seated xenoliths. They are mainly peridotites, although pyroxenites have also been described (e.g., Ancochea and Nixon, 1987; Villaseca et al., 2010; González-Jiménez et al., 2014; Villaseca et al., 2020; García Serrano et al., 2021). Lower crustal xenoliths are scarce and have only been found in the La Encomienda volcano (Fig. 1B). They have been recently classified in three groups according to their petrographic characteristics: (1) *meta*-noritic and *meta*-anorthositic, (2) aluminous felsic and (3) felsic granulites (Puelles et al., 2019). The latter study is focused on the zircon U–Pb geochronology and the deformation fabrics of the xenoliths. The U–Pb zircon data support an igneous origin for the *meta*-anorthositic protolith, with a crystallization age of 309 ± 3 Ma, whereas the aluminous granulite displays a peak at 288 ± 2 Ma (only 19% of analysed zircons), likely associated with the granulite-facies metamorphism, and an abundant group of older ages scattered in the range of ~350–600 Ma. On the other hand, the study of high-temperature microstructures in granulitic minerals has led these authors to suggest the possible existence of Late Variscan lithospheric shear zones that would have permitted the ascent of mantle components (represented by the *meta*-norites and *meta*-anorthosites) and their ponding at the base of the crust, thus promoting heating and melting (Puelles et al., 2019).

Outside the CIZ, other Cenozoic volcanoes also exhumed lower crustal granulitic xenoliths. In the Spanish SE Volcanic Field, at least the calc-alkaline dacitic El Hoyazo and the alkaline basaltic Tallante volcanoes entrained a felsic xenolith population (e.g, Álvarez-Valero and Waters, 2010; Bianchini et al., 2015, respectively), in the last case also accompanied by intermediate noritic cumulates and other mafic–ultramafic xenoliths. The Cofrentes volcano (Fig. 1), included in the Spanish Eastern Volcanic Region, carries *meta*-noritic granulite xenoliths within the lava flows of nephelinitic composition (Ancochea and Huertas, 2004). These xenoliths show petrographic features similar to those described in the Calatrava volcano. This volcano intruded in Mesozoic sedimentary rocks overlying a Variscan basement equivalent to that of the CIZ. Peridotite and scarce mafic granulite xenoliths have also been described in this volcano, not associated to peraluminous felsic types, which represent a marked contrast with respect to the SCS and CVF lower crustal xenolith populations. A preliminary study suggests a cumulate origin of the mafic protoliths and their later equilibration at granulite-facies conditions, at depths close to the Moho (García-Rodríguez et al., 2022).

3. Analytical methods

3.1. Mineral chemistry

The major element composition of minerals was determined at the *Centro de Microscopía Electrónica "Luis Bru" (Complutense University of Madrid)* using a JEOL JZA-8900 M electron microprobe with four wavelength dispersive spectrometers. Accelerating voltage was 15 kV and the electron beam current 20 nA, with a beam diameter of 5 μm. Counting time was 10 s on the peak and 5 s on each background position. The following mineral standards were used: sillimanite for Al; albite for Si and Na; almandine for Fe and Mn; kaersutite for Mg; microcline for K; ilmenite for Ti; Ni alloy for Ni and chromite for Cr. Corrections were made using the ZAF method. Analytical precision is 0.5%–6% for oxides with concentration >1.5 wt.% and <10% for oxides with concentration <1.5 wt.%.

Trace element analyses (REE, Ba, Rb, Sr, Th, U, Nb, Ta, Pb, Zr, Hf, Y, Sc, V, Co, Zn, Ni and Cr) in the main minerals were determined on > 90 μm-thick polished sections using an Agilent 8800 QQQ ICP-MS coupled to a Photon Machines Analyte Excite 193 laser source at the Instituto Andaluz de Ciencias de la Tierra (CSIC; Ganada). The diameter of the laser beam was 40–85 μm (depending on the mineral size) associated to repetition rates of 10–20 Hz and laser fluence at the target of ca. 8 J/cm^2. A 40–30 s gas blank was analysed first to establish the background, followed by 60 s measurements for the remainder of the analysis. The NIST 611 glass standard was used as primary reference material to calibrate relative element sensitivities for analyses of the silicate minerals. Precision and accuracy were assessed from repeated analyses of the BCR-2G standard and are estimated to be between 2% and 10% for most of the analysed trace elements. Each analysis was normalized to Si, Ca or K using concentrations determined by electron microprobe.

3.2. Whole-rock geochemistry and Sr-Nd isotopic ratios

Major and trace element analyses were carried out at ACTLABS (Ancaster, Ontario, Canada). The samples were melted using $LiBO_2$ and dissolved with HNO_3. Inductively coupled plasma atomic emission spectrometry (ICP-AES) was used for major element analysis, and trace elements were determined by inductively coupled plasma mass spectrometry (ICP-MS). Uncertainties in major elements range from 0.1% to 3%, except for MnO (5%–10%). The precision of ICP-MS analyses at low concentration levels has been evaluated from the repeated analyses of the international standards NIST-694, DNC-1, TDB-1, W-2, SY-4 and BIR-1. The precision for trace elements is in the range 1%–5%. More information on the procedure, precision and accuracy of ICP-MS analyses can be provided by Actlabs upon request.

Sr–Nd whole-rock isotopic analyses were carried out at the CAI de Geocronología y Geoquímica Isotópica (Complutense University of Madrid), using an automated VG Sector 54 multicollector thermal ionisation mass spectrometer. Analytical data were acquired in multidynamic mode. The analytical procedures used in this laboratory have been described elsewhere (Reyes et al., 1997). Repeated analyses of NBS 987 gave $^{87}Sr/^{86}Sr$ = 0.710243 ± 13 (2σ, n = 8) and the values of $^{143}Nd/^{144}Nd$ = 0.512108 ± 05 (2σ, n = 9) were obtained for the JNdi-1 Nd standard. The 2σ analytical errors are 0.01% for $^{87}Sr/^{86}Sr$ and 0.006% for $^{143}Nd/^{144}Nd$, which yield a 2σ error on ε_{Nd} calculation of ± 0.1. The BHVO-2 standard was used as a quality control yielding analysed mean values of $^{87}Sr/^{86}Sr$ = 0.703493 ± 0.00005 (2σ, n = 81) and $^{143}Nd/^{144}Nd$ = 0.513006 ± 0.00005 (2σ, n = 81) in agreement with the recommended values (Weis et al., 2006; Li et al., 2007).

3.3. Zircon U–Pb and Lu–Hf isotopic ratios and trace element composition

Zircons were separated using standard techniques and a representative selection (on the basis of their size and morphological features) was handpicked from each sample. These grains were mounted in epoxy resin for microanalytical analysis at the IBERSIMS laboratories (University of Granada, Spain), together with the reference zircons TEMORA 1, SL13 and REG. The mount was polished, and the zircon central portions were imaged with transmitted and reflected light, and with cathodoluminescence on a scanning electron microscope. Selected areas in the grains of seven samples (117449, 117450, 117455, U50, 77746, 77750 and 99187) were analysed for U, Th and Pb isotopes on the Sensitive High Resolution Ion Microprobe (SHRIMP II) with each analysis consisting of six scans through the relevant mass range. The primary beam, composed of $^{16}O^{16}O^{+}$, was set to an intensity of about 5 nA, with a 120 μm Kohler aperture, which generates 17 μm × 20 μm elliptical spots on the target. All calibration procedures were performed

on the standards included on the same mount. One TEMORA zircon standard was analysed for every-four unknown analyses. Data was reduced using the SHRIMPTOOLS software (available from https://www.ugr.es/~fbea), specifically developed for IBERSIMS by Fernando Bea. More details can be found in https://www.ugr.es/~ibersims/ibersims/Sample_analysis_and_methods.html. Pb/U ratios were normalised relative to a value of 0.06683 for the $^{206}Pb/^{238}U$ ratio of the TEMORA reference zircon, equivalent to an age of 417 ± 1 Ma (IDTIMS in zircon; Black et al., 2003). Concentration data was normalised against zircon standard SL13 (210 ppm U, Black et al., 2004). Ages younger than 1000 Ma are 204-corrected $^{206}Pb/^{238}U$, whereas older ages are 204-corrected $^{207}Pb/^{206}Pb$.

The Lu–Hf zircon isotope ratios were obtained using an ASI/Applied Spectrum RESOlution Excimer laser ablation system coupled to a NPII multi-collector ICP-MS. Where the grain size permitted it, a 60 μm spot size has been used, overlapping with the ablation spot for the trace elements; the repetition rate was 7 Hz and the fluence 5 J/cm^{-2}. Each analysis consisted of a 15 s blank followed by a 60 s ablation signal. Details for the Lu-Hf correction procedures can be found in Jacobs et al. (2017). The Mud Tank, LV-11 and Temora-2 zircons were analyzed for quality control and gave results that are within uncertainty of accepted values ($^{176}Hf/^{177}Hf$ average and 1 sigma: 0.282503 ± 0.000013, 0.282809 ± 0.000020, 0.282676 ± 0.000017, respectively). The initial epsilon Hf isotopic value ($\varepsilon_{Hf}(t)$) was calculated using the decay constant of ^{176}Lu of 1.867 × 10^{-11} yr^{-1} (Söderlund et al., 2004), and ratios for the chondritic uniform reservoir (CHUR) of $^{176}Hf/^{177}Hf$ = 0.282785 and $^{176}Lu/^{177}Hf$ = 0.0336 (Bouvier et al., 2008).

Trace element concentrations in zircon were obtained at the University of Johannesburg, using an ASI/Applied Spectrum RESOlution Excimer laser ablation system coupled to a ThermoScientific iCap quadrupole ICP-MS. The spot size used was 30 μm with a repetition rate of 4 Hz, and a fluence of 1.4 J/cm^2. The spots were put in the same CL zone as where the U–Pb had taken place before. Quantification was done using NIST610 glass as a primary reference material, using Si as an internal standard, in the program LADR (Norsci.com). Quality control was based on the analysis of zircon GJ-1 of which the obtained concentrations are generally within 15% of those reported by Piazolo et al. (2017), apart from P, which came out at 83 rather than 30 ppm. Importantly, the value for Ti opbtained (3.5 ± 0.3 ppm) is within uncertainty of the value reported by Piazolo et al. (2017).

4. Petrography

The SCS granulite xenoliths are included in Permian mafic alkaline dykes and represent fragments from the lower crust beneath the Spanish Central System. A detailed petrographic characterization of these xenoliths (including three out of the four samples studied in this work: U50, 77746 and 77750) can be found in Villaseca et al. (1999), so just a brief summary will be presented here. The most abundant xenoliths are metaigneous felsic types (~90 vol.%) and metapelitic granulites (~9 vol.%), although intermediate charnockitic types (~1 vol.%) have also been described (e.g., Villaseca et al., 2007b) (Fig. 1D). They show granoblastic textures and commonly display compositional banding with quartz–feldspar-rich and garnet ± sillimanite-rich bands. Orthopyroxene is found in some garnet-bearing felsic types. Phlogopite is present only in the felsic granulites, whereas clinopyroxene is restricted to the charnockites. Kelyphitic coronas around garnet are frequent and composed of a microcrystalline symplectitic aggregate of spinel, orthopyroxene, feldspars and scarce quartz. Common accessory phases are rutile, ilmenite, apatite, zircon, monazite, graphite and sulphides. Samples 77746 and 77750 are metapelitic types, characterised by abundant garnet (22%–26%) and sillimanite (8%–13%), whereas samples U50 and 99187 can be classified as metaigneous felsic granulites with accessory phlogopite and no sillimanite.

The Calatrava granulite xenoliths can be grouped in three different types according to their petrographic characteristics (Fig. 1D; Table 1): type-I charnockitic granulites (samples 117449 and 117451), type-II garnet-bearing felsic granulites (samples 117453, 117454 and 117455) and type-III metagranitoids (samples 117448, 117450 and 117452).

The type-I charnockitic xenoliths have an elongated shape and sizes ranging from 6 to 10 cm. They show a fine- to medium-grained inequigranular granoblastic texture (Fig. 2A, B). Slight banding is also observed, with feldspathic and opx–grt-rich domains, whereas oriented biotite crystals impart a slight foliation (Fig. 2B). The main minerals are plagioclase (67–70 vol.%), pale-brown orthopyroxene (21–25 vol.%), garnet (0–7 vol.%) and biotite (0–8 vol.%). Biotite has only been found in sample 117451, whereas garnet is only present in sample 117449. Kelyphitic coronas develop around garnet crystals. Accessory phases are quartz (with rutile needle inclusions), apatite, ilmenite, magnetite, rutile grains, zircon and monazite. Although the modal composition of these rocks suggests their classification as *meta*-norites *s.l.*, the plagioclase composition (mainly andesine; Puelles et al., 2019), low colour index (<35%), peraluminous chemistry and the presence of accessory quartz, lead to a more likely classification as orthopyroxene diorites of the charnockitic group (Le Maitre et al., 2002).

Type-II garnet-bearing granulite xenoliths are rounded to elongated in shape and their size ranges from 4 to 7 cm. They display medium-grained inequigranular granoblastic textures (Fig. 2C, D) and a slight banding marked by garnet-rich domains. The main minerals are plagioclase (27–45 vol.%), K-feldspar (14–40 vol.%), quartz (20–28 vol.%) and garnet (8–20 vol.%) (Table 1). Biotite and sillimanite are also present in proportions below 2 vol.%, and other accessory phases are apatite, ilmenite, rutile and zircon. Kelyphitic coronas are present around garnet crystals.

Type-III metagranitoid xenoliths display circular to ovoid shapes, and sizes ranging from 7.5 to 14 cm. They show inequigranular textures with a medium to fine-grained matrix and a poor development of triple junctions between minerals (Fig. 2E, F). The main minerals and their abundance (in volume) are plagioclase (24–74 vol.%), K-feldspar (5–50 vol.%), quartz (15–25 vol.%) and biotite (<1–5 vol.%). According to these mineral proportions (recommendations of the International Union of Geological Sciences; Le Maitre et al., 2002), the rocks can be classified as metagranites (samples 117448 and 117450) and metatonalite (sample 117452). K-feldspar is interstitial, but it occasionally forms large crystals (up to 1.5 cm) intergrown with quartz. In these cases, K-feldspar shows simple twinning, perthite exsolution and may include plagioclase crystals. Myrmekitic intergrowths are found where the K-feldspar is in contact with plagioclase. The observed accessory phases are apatite and zircon. No sillimanite or garnet occur in this xenolith type.

All the studied xenoliths show signs of deformation (i.e., cracks, undulatory extinction and tapered twinning in plagioclase), and local infiltration of the host mafic melt and formation of secondary calcite and zeolites.

Taking into account the above petrographic characteristics, two of these types of xenoliths can be correlated to those described by Puelles et al. (2019) for the same volcano. Our type-I xenoliths correspond to their *meta*-norites, although *meta*-anorthosite samples (or most probably, plagioclase-rich *meta*-diorites) have not been found in our sampling. Our type-II xenoliths correlate with their felsic granulites, which likely represent the psammitic variety of a wider suite of metasedimentary felsic granulites, including a third xenolith type (metapelitic grt-sill-rich aluminous granulites)

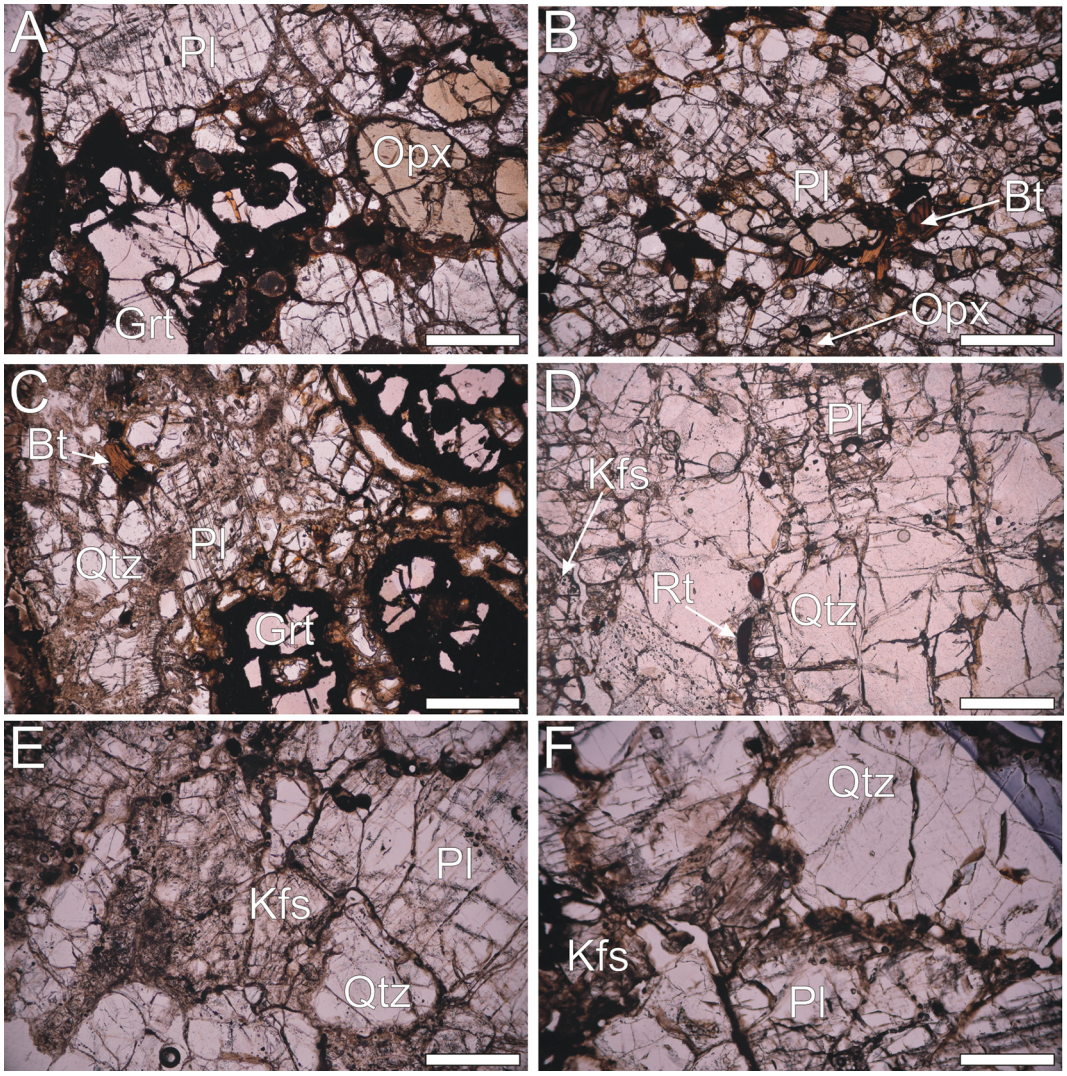

Fig. 2. Plane polarized light images showing the main textures of the Calatrava granulite xenoliths. (A, B) Charnockitic granulites (samples 117449 and 117451, respectively); (C, D) garnet felsic granulites (samples 117453 and 117455, respectively); (E, F) metagranitoids (samples 117448 and 117450, respectively). The white bar represents 1 mm.

distinguished by Puelles et al. (2019). Our type-III metagranitoid xenoliths have no known equivalent in previous samplings.

5. Mineral chemistry

The mineral chemistry of the SCS granulites has already been discussed in previous works (Villaseca et al., 1999, 2007a, 2007b), so below we focus the description on the Calatrava samples, with the only exception of zircon, for which new analyses from both areas have been obtained.

5.1. Feldspars

Feldspar major and trace element compositions can be found in Supplementary Data (Tables S1A and S2A). Plagioclase from type-I xenoliths displays the highest Ca contents, with up to An_{75} in a plagioclase core of the *meta*-norite 117451, although most crystals are in the range $An_{39–55}$ (Supplementary Data, Fig. S1A). This composition is similar to that of plagioclase crystals from charnockite xenoliths from the SCS (Villaseca et al., 2007b), but slightly higher in anortite content when compared to previous data of Puelles et al. (2019) in the same xenolith type (An_{34}). Type-III plagioclase is mostly andesine and oligoclase ($An_{13–36}$) and those from type-II xenoliths overlap with them within a narrower range ($An_{29–33}$). Na_2O concentration rises towards the less calcic plagioclases (from 2.8 to 9.7 wt.%) and K_2O is usually below 0.7 wt.% (except for a few type III plagioclase crystals, reaching up to 2.2 wt.%). These low K contents contrast with the high K (up to 5 wt.%) and correlative orthoclase composition of plagioclases from some SCS felsic granulite xenoliths (Or up to 30 mol.%) that show a typical antiperthitic appearance (e.g., Fig. 6a in Villaseca et al., 2007a).

Plagioclase trace element contents are very variable between xenolith types. As a whole, calcic plagioclase from the charnockitic granulite 117449 exhibits high Sr (780–875 ppm), Ba (75–131 ppm) and LREE values (e.g., La = 48–56 ppm), and shows steep chondrite-normalised patters (La_N/Yb_N = ~6000–9500) and positive Eu anomaly (Supplementary Data, Fig. S1B, C). LREE patterns in type-II plagioclases have a positive slope from La to Nd but are considerably lower than those of charnockitic plagioclases. The very low trace element contents of type-III plagioclases do not allow a reliable characterization. K-feldspar composition is similar in the two xenolith types in which it is present, and corresponds to $Or_{63–95}$ (Supplementary Data, Fig. S1A). Sr, Ba and Pb values are much higher in type-II K-feldspar (650–710 ppm, 2700–3100 ppm and 630–650 ppm, respectively), than in type-III (173–180 ppm, 22–34 ppm and < 42 ppm, respectively)

(Supplementary Data, Fig. S1B). REE display fractionated normalised pattern in all cases and a positive Eu anomaly, but type-III feldspar stands out due to higher LREE (La, Ce, Pr, Nd and Eu) abundances (Supplementary Data, Fig. S1C). The low LREE contents of feldspars of these CVF felsic granulites are remarkable when compared to those of the SCS felsic xenoliths (Supplementary Data, Fig. S1D) (Villaseca et al., 2007a).

5.2. Orthopyroxene

Orthopyroxene is only present in charnockitic (type-I) xenoliths, where it shows a variable composition (Supplementary Data, Table S1B) characterised by moderate Mg# (0.57–0.65). Orthopyroxene from sample 117449 is less magnesian than that from sample 117451, and this lowering of the Mg# value is accompanied by a decrease in Al and Ti and an increase in Si, Ca and Mn concentration (Supplementary Data, Fig. S2A). Charnockitic diorite 117451 has an orthopyroxene major element composition very similar to that from the SCS charnockites, whereas *meta*-diorite 117449 has a low-Ca, high-Al orthopyroxene (Supplementary Data, Fig. S2B) similar in composition to that of the SCS garnet-bearing felsic types (type 2a of Villaseca et al., 2007b). On the contrary, no orthopyroxene has been found in any other type of CVF felsic xenolith.

The trace element contents determined in sample 117449 are moderate for transition metals, such as V (up to 812–902 ppm) and Cr (up to 200–489 ppm) and very low for the rest of elements (Supplementary Data, Table S2B). REE chondrite-normalised patterns display flat or slightly positive HREE fractionation with marked negative Eu anomaly and abundances in the range 0.1–10 × chondrite (Supplementary Data, Fig. S2C).

5.3. Garnet

The major element composition of the CVF granulitic garnet exhibits only a minor variation between xenoliths (Supplementary Data, Table S1C) and corresponds to the almandine–pyrope series (Py_{30-44}). Garnet composition is homogeneous within a single sample, and the main difference between groups is the slightly higher Ca values shown by the charnockitic granulites with respect to the type-II garnet felsic granulites (Supplementary Data, Fig. S3A). Moreover, garnet from charnockite 117449 plots within the compositional field of garnet from SCS felsic metaigneous xenoliths, whereas garnet from type-II felsic granulites display a composition similar to garnet from all felsic SCS xenoliths (either metaigneous or metapelitic; Villaseca et al., 1999). Higher Mn and lower Cr contents are present in garnets with lower Mg# (Supplementary Data, Fig. S3A). No significant zoning has been observed, similarly to garnet in the SCS felsic xenoliths (e.g., Orejana et al., 2011). Most trace elements show low concentrations, with the exception of some transition metals (e.g., Co, V, Cr), Zr, Y and HREE (Supplementary Data, Table S2C). Nevertheless, they show marked lower Y and Zr contents when compared to SCS granulitic garnets (Villaseca et al., 2007a; Orejana et al., 2011) (Supplementary Data, Fig. S3C).

The garnet chondrite-normalised REE patterns display typical low LREE abundances and negative Eu anomaly. HREE show a more variable behaviour, with depletion towards Lu in the charnockitic granulite and higher and flatter HREE shapes in the garnet felsic granulites (Supplementary Data, Fig. S3B). These REE patterns are very similar in shape and abundance to those from the SCS felsic xenoliths (e.g., Orejana et al., 2011).

5.4. Biotite/phlogopite

The major element composition of mica (Supplementary Data, Table S1D) has been analysed in all xenolith types and this mineral can be classified mainly as biotite, following the criteria of Heinrich et al. (1953), although phlogopite is present in one metasedimentary granulite (117455). As a whole, its composition is heterogeneous, but only small variations are observed within a single xenolith. A broad tendency to lower Si, Na and F, and higher Al, K and Cl, can be identified towards more evolved compositions (Supplementary Data, Fig. S4A, B). No significant differences between xenolith types are apparent, with the exception of the lower Al values shown by biotite from the charnockitic granulite 117451 and the slightly higher TiO_2 contents in the charnockites and *meta*-granitoid xenoliths (up to 5.4 wt.%, Supplementary Data, Table S1D). Nevertheless, even higher TiO_2 contents (up to 7.8 wt.%) are characteristic of phlogopite from the SCS felsic xenoliths (Villaseca et al., 1999 and unpublished data).

Trace elements have been determined in types II and III xenoliths and they yield contrasting results (Supplementary Data, Table S2D). Biotite from the metagranite shows high abundance of most elements (Rb, Sr, Pb, Nb, Ta, Y, Sc, Co, Ni and REE), only displaying low V concentrations (Supplementary Data, Fig. S4C). The higher REE values in biotite from the metagranite are reflected in slightly fractionated chondrite-normalised patterns with La abundances in the range of ~ 30–300 × chondrite, whereas those of phlogopite from the metasedimentary xenolith are below 1 (Supplementary Data, Fig. S4D).

5.5. Zircon

Zircon trace element contents from the analysed samples are very heterogeneous (Supplementary Data, Table S3), but a broad distinction that can be made between inherited cores, which usually display oscillatory zoning, and rounded grains and rims, either unzoned or with sector zoning. Most inherited zircons show chondrite-normalised REE patterns with pronounced positive Ce anomalies and steep mid to heavy-REE positive slopes (Gd_N/Yb_N < ~0.15) (Fig. 3A). They are also characterised by variable Nb (1–25 ppm), Ta (0.3–7.9 ppm) and Y (140–5495 ppm) concentrations. In contrast to the inherited cores, zircons of metamorphic origin (homogeneous grains and rims) reveal a more complex composition. They usually show nearly flat mid- to heavy-REE patterns (Gd_N/Yb_N mostly in the range 0.25–5.4), less pronounced Ce peaks and lower Nb, Ta and Y concentrations, although some zircons from the Calatrava samples (117449, 117450 and 117455) resemble the composition of the inherited cores (Fig. 3). Ti concentrations range from 16 to 87 ppm in types II and III xenoliths, whereas zircon from charnockite 117449 has a slightly wider range of 24 to 142 ppm. A small number of inherited grains reaches higher values, up to 345 ppm (Supplementary Data, Table S3). Zircons of the SCS felsic xenoliths have a higher range of Ti contents (47–142 ppm) when compared to those of the CVF types II and III (Supplementary Data, Table S3).

5.6. Rutile

Only rutile from the metasedimentary granulite 117455 could be analysed, due to the small size or absence of rutile in other xenolith types. The trace elements showing higher concentrations in rutile are mainly HFSE, such as Zr (710–3900 ppm), Nb (1730–2290 ppm), Hf (26–74 ppm) and Ta (40–62 ppm), together with V (3410–4276 ppm), Cr (1087–1820 ppm) and U (10–18 ppm) (Supplementary Data, Table S2E). The Zr and U contents of rutile from this granulite xenolith are lower than those from the SCS felsic xenoliths (Villaseca et al., 2007a).

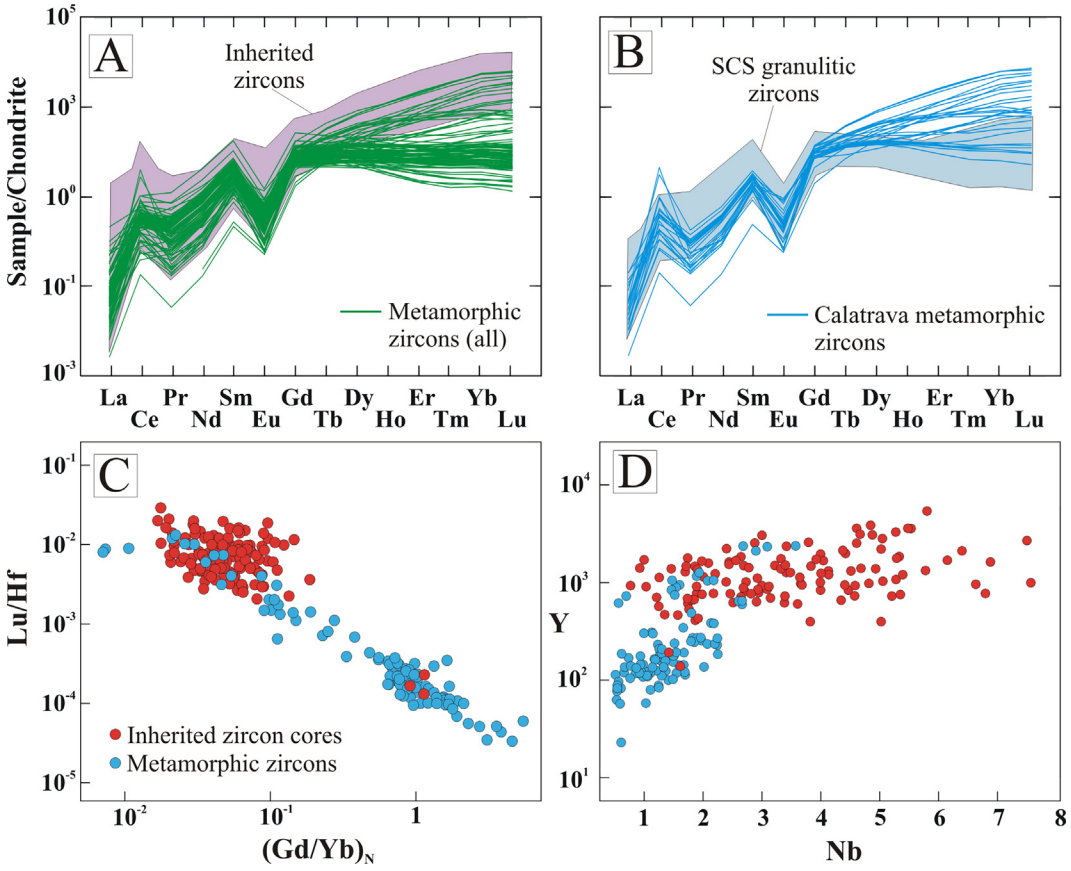

Fig. 3. Trace element composition of zircons from the SCS and Calatrava granulite xenoliths: chondrite-normalised REE contents of all zircons (A) and metamorphic (granulite) zircons (B), and Lu/Hf and $(Gd/Yb)_N$ ratios (C) and Nb–Y contents (ppm) (D) of inherited zircon cores vs metamorphic zircons. Chondrite values after Sun and McDonough (1989).

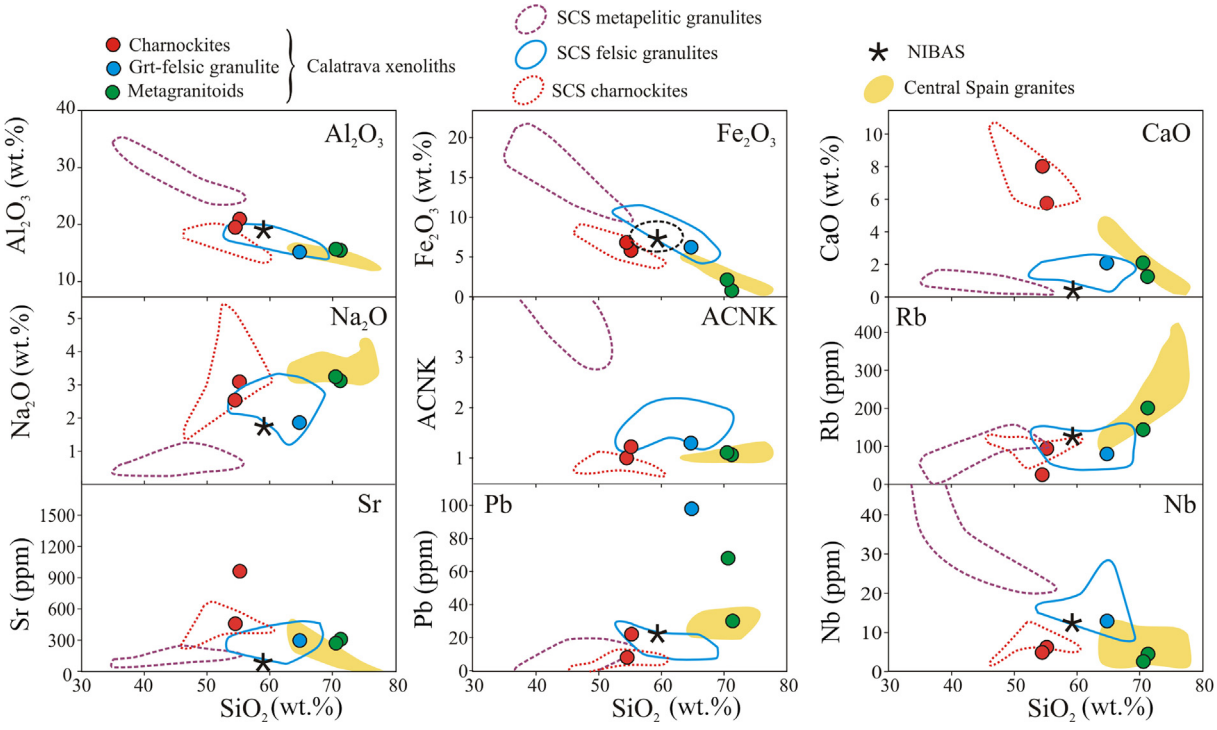

Fig. 4. Whole-rock geochemistry (selected elements) of the Calatrava granulite xenoliths. Several data have also plotted for comparison: Central Spain granites taken from Villaseca et al. (1998), Donaire et al. (1999) and Errandonea et al. (2017); SCS metapelitic, felsic and charnockitic granulites after Villaseca et al. (1999, 2007b); NIBAS (Neoproterozoic Iberian Average Shale) is representative of the Schist Greywacke Complex (SGC) metasediment composition and has been taken from Ugidos et al. (2010).

6. Whole-rock chemistry

6.1. Major and trace elements

Clear differences in major and trace element concentrations exist between the three CVF xenolith types (Table 2). The charnockitic (type-I) and metagranitoid (type-III) granulites represent contrasting compositional poles, the first displaying lower SiO_2 (~54–55 wt.%), Na_2O, K_2O, Rb and Pb contents and the latter showing the lowest values for MgO, CaO, TiO_2, Cr, Ni and Sr (Fig. 4). The garnet granulite (type-II) is felsic in composition (SiO_2 ~65 wt.%) and plots in an intermediate position (except for the low Na and relatively high K, Fe, Ti, Pb and Nb concentrations). All xenoliths exhibit a moderate to high alumina saturation index (ACNK in the range 1.1–1.3), with the metasedimentary felsic granulites being the most peraluminous (Table 2). The chondrite-normalised REE abundances of CFV granulite xenoliths are fairly variable, but yield similar patterns with moderate to strong LREE fractionation and almost flat HREE (Fig. 5A). Eu anomalies are positive in the two samples with lower REE contents and negative in the rest of samples. As a whole, the primitive mantle-normalised trace element patterns are also heterogeneous and characterised by a moderate LILE enrichment, Nb–Ta, P and Ti throughs and positive Pb and Sr anomalies (Fig. 5B).

Fig. 4 displays the composition of lower crustal xenolith suites from the nearby region of the Spanish Central System (SCS), where diverse lithologies have also been described (Villaseca et al., 1999, 2007b). When comparing the composition of the La Encomienda xenoliths with those from the SCS, it is apparent that the CVF garnet felsic granulite shows a major and trace element composition very similar to that of the SCS felsic granulites, with the exception of higher Zr and Pb contents, and that the CVF charnockitic granulites closely resemble the SCS charnockites. On the other hand, the metagranitoids do not match any of the SCS granulite xenoliths, because of their extremely SiO_2-rich character (Fig. 4), but show a composition equivalent to that of evolved granites.

Table 2
Whole-rock composition (major and trace elements) of granulite xenoliths from the Calatrava Volcanic Field.[1]

Sample	117451	117449	117455	117450	117448
Type[2]	I	I	II	III	III
SiO_2	54.48	55.19	64.75	70.52	71.25
TiO_2	1.05	0.80	0.81	0.17	0.12
Al_2O_3	19.51	20.94	15.15	15.68	15.46
Fe_2O_3	6.82	5.82	6.23	2.14	0.76
MnO	0.11	0.09	0.09	0.08	0.01
MgO	3.80	2.28	2.52	0.52	0.48
CaO	8.01	5.75	2.08	2.09	1.25
Na_2O	2.54	3.09	1.86	3.24	3.12
K_2O	0.71	1.46	4.48	4.66	6.60
P_2O_5	0.13	0.14	0.10	0.09	0.19
LOI	3.68	5.06	1.73	1.24	0.98
Total	100.80	100.60	99.81	100.40	100.20
ACNK[3]	1.0	1.2	1.3	1.1	1.1
Mg#	0.69	0.61	0.62	0.49	0.71
Rb	25.00	94.00	80	144.00	201
Ba	179	1227	1155	2572	885
Cs	0.30	0.30	0.30	0.70	1.60
Sr	457	961	295	270	307
Pb	8.00	22.0	98	68.0	30
Th	1.70	137	8.78	13.50	1.83
U	1.21	3.56	1.04	1.46	1.66
Zr	43	606	377	83	29
Nb	4.90	6.20	12.9	2.60	4.50
Y	5.30	29.6	26.6	24.0	2.90
Co	21.0	15.0	27.0	4.00	1.00
V	134	83.0	104	19.0	7.00
Ni	30.0	40.0	40.0	20.0	20.0
Cr	70.0	50.0	90.0	20.0	20.0
Ga	22.0	37.0	22.0	18.0	22.0
Ta	0.46	0.15	0.72	0.21	0.78
Hf	1.00	14.70	9.30	2.30	0.80
La	8.44	307	55.00	25.6	8.72
Ce	16.6	574	115.0	53.2	16.9
Pr	2.05	65.6	12.4	6.44	1.75
Nd	7.49	218	43.7	22.5	5.71
Sm	1.56	30.2	7.45	4.61	1.04
Eu	0.90	3.03	1.66	0.85	0.70
Gd	1.38	15.4	6.15	3.90	0.89
Tb	0.20	1.50	0.84	0.63	0.13
Dy	1.11	6.88	5.05	4.14	0.66
Ho	0.20	1.16	0.98	0.88	0.10
Er	0.55	2.83	3.09	2.57	0.24
Tm	0.08	0.33	0.45	0.36	0.03
Yb	0.50	1.89	3.17	2.30	0.21
Lu	0.08	0.29	0.52	0.32	0.03

[1] Major and trace elements concentrations in wt.% and ppm, respectively.
[2] I: Charnockitic granulites; II: garnet felsic granulites; III: metagranitoids.
[3] ACNK = $[Al_2O_3/(CaO + Na_2O + K_2O)]$ in molecular values.

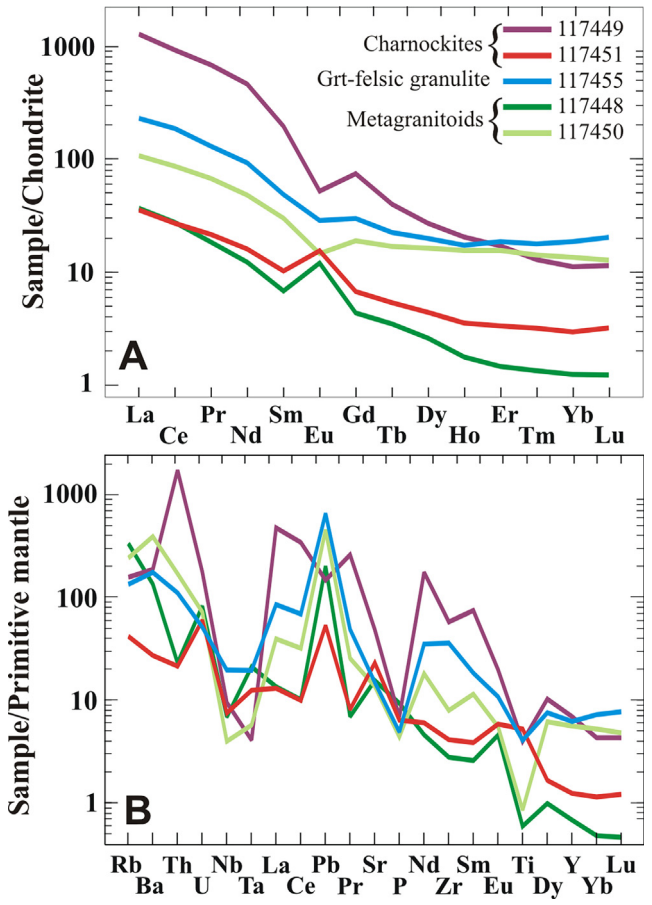

Fig. 5. Chondrite-normalised (A) and primitive mantle-normalised (B) trace element composition of the Calatrava granulite xenoliths. Chondrite and primitive mantle values after Sun and McDonough (1989) and McDonough and Sun (1995), respectively.

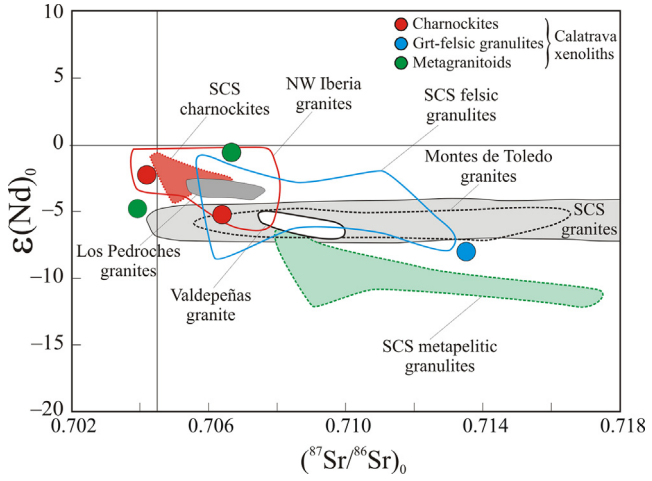

Fig. 6. Sr–Nd isotope composition of the Calatrava granulite xenoliths. The compositional fields corresponding to NW Iberia granites (Villaseca et al., 2009), Los Pedroches granites (Donaire et al., 1999; Carracedo et al., 2009 and references therein), Valdepeñas granite (Errandonea et al., 2017), Montes de Toledo granites (Merino–Martínez et al., 2014) and SCS granites (Villaseca et al., 1998) have been represented for comparison. The fields of the SCS granulite xenoliths (charnockitic, felsic and metapelitic) are taken from Villaseca et al. (1999, 2007b).

6.2. Sr–Nd isotopes

The Sr and Nd isotopic ratios of the CVF xenoliths, calculated back to 309 Ma, also display differences between groups (Table 3). The felsic garnet granulite shows the most radiogenic values, with $^{87}Sr/^{86}Sr$ = 0.7135 and ε_{Nd} = −8. This composition is somewhat intermediate between the fields of the SCS felsic and metapelitic granulite xenoliths (Fig. 6). On the contrary, both type-I (charnockites) and type-III (metagranitoids) xenoliths exhibit more depleted values, with overlapping $^{87}Sr/^{86}Sr$ = 0.7039–0.7066 and ε_{Nd} = −0.6 to −5.2. These latter two groups have an isotopic composition very similar to that of the lower crust SCS charnockites and partially overlap the field of SCS *meta*-igneous felsic xenoliths. A clear similitude also exists with respect to several CIZ granite batholiths, including those from southern CIZ (Los Pedroches batholith) and NW Iberia (Fig. 6).

7. U–Pb geochronology

7.1. Zircon description

The size, morphology and textural features of zircons from samples 117449, 117450 and 117455 from the La Encomienda volcano (CVF), and samples U50, 77746, 77750 and 99187 from the Spanish Central System (SCS), were studied by transmitted and reflected microscopy and CL imaging in 108, 95, 113, 67, 95, 149 and 120 grains, respectively. The CL internal structure from representative grains is shown in Fig. 7.

Zircons mainly consist of colourless or yellowish crystals with variable shape. Rounded and equant multifaceted to slightly elongated grains predominate in the SCS granulites and in sample 117455 from Calatrava, whereas long or stubby prisms are much more abundant in samples 117449 and 117450 from Calatrava. They range in size from 50 to 300 μm, and the most elongated crystals show aspect ratios of 1:5. CL imaging of SCS granulite zircons reveals a variable proportion of grains with inherited cores, ranging from 0% (77746) to 52% (77750). These cores are usually subhedral prisms or display an anhedral rounded shape. They may show a variety of internal textures: oscillatory zoning, convoluted zoning, sector zoning and bright wide bands, or they may be unzoned, either dark or bright (Fig. 7). These cores are usually enclosed by homogeneous rims. SCS rounded zircons may be unzoned or display sector zoning. The Calatrava samples stand out for their abundance of inherited zircon cores: 70% of the grains in sample 117450 and up to 90% in sample 117449 (Table 1). CL images reveal a predominance of oscillatory zoning in zircon cores of samples 117449 and 117450, while more variability appears in sample 117455 (oscillatory zoning, sector zoning, homogeneous areas, etc). Zircon rims in the Calatrava samples are usually thin and there are a small proportion of equant unzoned zircons. Textures likely associated with secondary processes are relatively common in zircon cores from all samples: convoluted zoning, chaotic zoning, widening of bands and local recrystallization (e.g., Corfu et al., 2003).

7.2. Analytical results

A total of 489 crystals were analysed for U–Pb isotopes, some of them in several places (core and rim), resulting in 587 analyses in all samples (Supplementary Data, Table S4). The ages obtained have been filtered, excluding results with high common Pb (>1.1%) and high degree of discordancy (>10%), in order to get a reliable dataset and provide a meaningful discussion. Hereafter,

Table 3
Sr–Nd isotopic composition of Calatrava granulite xenoliths.

Sample	Xenolith type	Rb (ppm)	Sr (ppm)	$^{87}Rb/^{86}Sr$	$^{87}Sr/^{86}Sr \pm (2\sigma)$	$^{87}Sr/^{86}Sr_{309\ Ma}$	Sm (ppm)	Nd (ppm)	$^{147}Sm/^{144}Nd$	$^{143}Nd/^{144}Nd \pm (2\sigma)$	$\varepsilon_{Nd,309\ Ma}$
117449	I	94	961	0.28	0.707646 ± 06	0.70640	30.2	218.0	0.084	0.512141 ± 02	−5.2
117451	I	25	457	0.16	0.704901 ± 08	0.70420	1.6	7.5	0.126	0.512379 ± 04	−2.3
117455	II	80	295	0.79	0.716978 ± 04	0.71352	7.5	43.7	0.103	0.512038 ± 04	−8.0
117448	III	201	307	1.90	0.715016 ± 04	0.70668	1.0	5.7	0.110	0.512433 ± 06	−0.6
117450	III	114	270	1.22	0.709308 ± 06	0.70393	4.6	22.5	0.124	0.512245 ± 04	−4.8

Rb, Sr, Sm and Nd concentrations determined by ICP-MS.

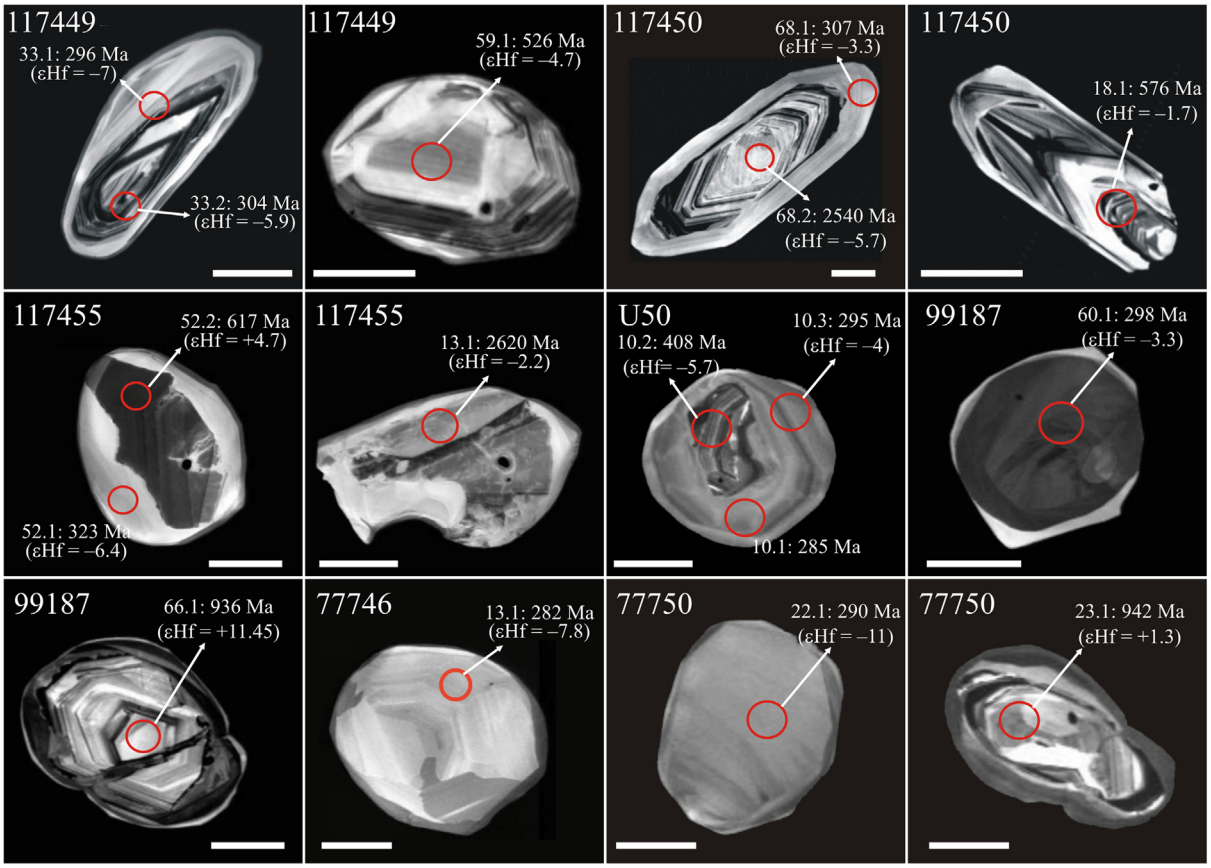

Fig. 7. CL images of representative zircon grains from the SCS and Calatrava granulite xenoliths, showing the analysed spots, the U–Pb age (Ma) and ε_{Hf} value. The white bar represents 50 μm.

any mention of number of analyses refers to filtered good-quality data. Due to data dispersion, no concordia ages could be calculated for those age populations likely associated to a specific magmatic of metamorphic event. In these cases, a weighted average $^{206}Pb/^{238}U$ age or a Tuffzirc age have been obtained. The Tuffzirc algorithm (Ludwig and Mundil, 2002) can get a reliable result from complex age populations with slight positive and negative age biases. This method has been used mainly when the weighted average age was accompanied by high uncertainty. For zircons from the SCS granulites, all data younger than the age of the host mafic dyke (~270 Ma; Orejana et al., 2020) have been excluded from the above calculations and the probability density diagrams.

7.2.1. Sample 117449 (CVF charnockitic granulite)

Zircon cores (n = 89) with oscillatory zoning or secondary textures (e.g., convoluted zoning) display ages mostly restricted to a Permo–Carboniferous range (277–355 Ma) with a peak located around 315 Ma (Fig. 8A1, D and E). The only exception are two older ages (441 Ma and 526 Ma). Rims are usually thin bands around large cores, and their ages (n = 17) broadly overlap the range of cores but shifted towards the younger values (~277–318 Ma). Their distribution reaches its higher abundance between 280 Ma and 297 Ma. The relative concentration of ages in a narrow range and extremely scarce older inherited zircons (2%), both from core and rim data, suggests that zircon cores represent the magmatic age of the rock (consistent with the predominance of oscillatory zoning patterns), whereas rims formed afterwards during a subsequent recrystallization event. We have used the TuffZirc method and obtained an age of 298.9 (+5.6/−3.6) Ma for the rims and 313.5 (+4.1/−1.9) Ma for the zircon cores (Fig. 8A2 and A3); the latter overlap within uncertainty with the age of 309 ± 3 Ma provided for equivalent xenoliths (*meta*-anorthosites) from the same Calatrava volcano (Puelles et al., 2019).

7.2.2. Sample 117455 (CVF garnet felsic granulite)

Cores analysed in this sample (n = 67) provide a more heterogeneous age distribution, characterised by Paleozoic (433–536 Ma; 32%), Ediacaran–Cryogenian (543–661 Ma; 41%), Tonian (750–

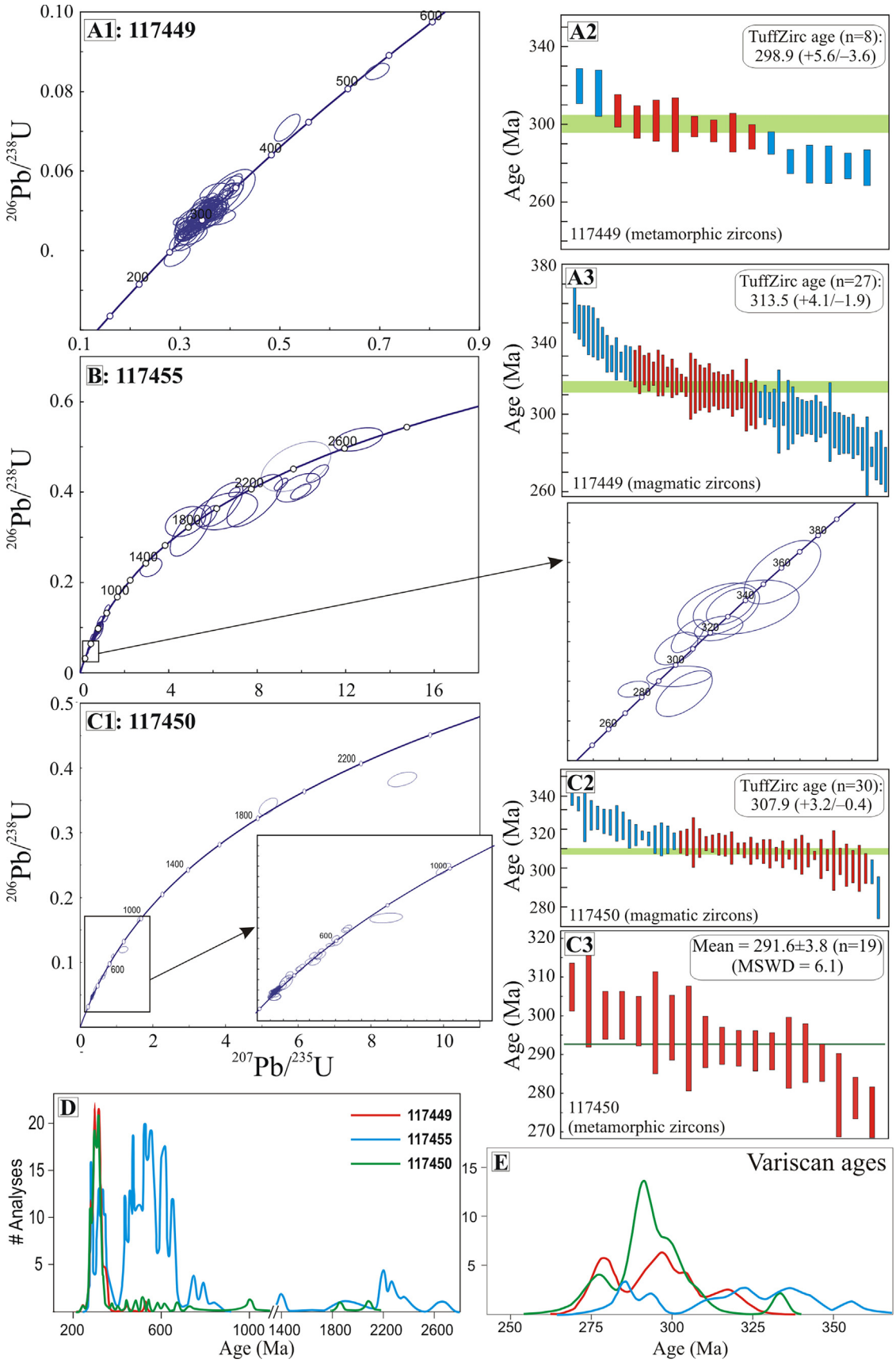
A1: 117449
B: 117455
C1: 117450
206Pb/238U
207Pb/235U
A2
TuffZirc age (n=8):
298.9 (+5.6/–3.6)
117449 (metamorphic zircons)
A3
TuffZirc age (n=27):
313.5 (+4.1/–1.9)
117449 (magmatic zircons)
C2
TuffZirc age (n=30):
307.9 (+3.2/–0.4)
117450 (magmatic zircons)
C3
Mean = 291.6±3.8 (n=19)
(MSWD = 6.1)
117450
(metamorphic zircons)
Age (Ma)
D
117449
117455
117450
Analyses
Age (Ma)
E
Variscan ages
Age (Ma)

840 Ma; 6%), Paleoproterozoic (1618–2433 Ma; 15%) and Neoarchean (2601–2656 Ma; 6%) ages (Fig. 8B, D). These data do not allow a straightforward conclusion with respect to the igneous or sedimentary origin of the host protolith (see discussion section), although the abundance of Paleozoic and Neoproterozoic zircon cores suggest a link to Cadomian basement protoliths. Rims consist of bright thin bands or wider recrystallised areas which show ages in the range 282–377 Ma (Fig. 8B, E). No reliable ages have been obtained for the Variscan granulitic event. An imprecise weighted average age of 304 ± 15 Ma is obtained using the scarce number of rim analyses (n = 12), which present an irregular bimodal distribution with peaks situated at 282–293 Ma and 315–340 Ma. This xenolith yielded the maximum relative abundance of zircon inheritances (85%) of the CVF sampling (Table 1).

7.2.3. Sample 117450 (CVF metagranitic granulite)

The prismatic shape of zircons from this sample and oscillatory zoning point to a magmatic origin, whereas rim textures support a later stage of recrystallization. The age distribution shown by the cores (n = 73) is in accordance with this possibility, as a vast majority (70%) is restricted to the range of ~285–335 Ma (Fig. 8C1, D). A small number (<30%) of older cores displays mainly Late Paleozoic to Early Neoproterozoic ages, reaching up to Neoarchean. The thin rims analysed in this sample (n = 21) yield younger and overlapping ages (275–307 Ma), with respect to the zircon cores (Fig. 8E). The TuffZirc algorithm calculates an age of 307.9 (+3.2/–0.4) Ma for the Permo–Carboniferous cores and 293.2 (+5.4/–2.4) Ma for the surrounding rims (Fig. 8C2). The latter date is equivalent to the calculated weighted average age (291.6 ± 3.8 Ma; MSWD = 6.1) for the same rims (Fig. 8C3).

7.2.4. Sample U50 (SCS felsic granulite)

The mostly rounded zircon grains of this sample exhibit clear recrystallization CL textures, typical of high-grade metamorphic rocks (Corfu et al., 2003). The anhedral cores (n = 29) include an abundant Permo–Carboniferous population with peaks at 270–295 Ma and 322–333 Ma, together with subordinate Neoproterozoic zircons (Fig. 9A, E, F). Analyses performed in homogeneous dark zircons and rims (n = 27) reveal a range (256–301 Ma) very similar to the youngest one found in the cores (Fig. 9F). The abundance of inheritances with Permian and Carboniferous ages, some of them overlapping those of rims, is an indication that a strong modification of zircon U–Pb isotopic ratios likely occurred because of granulitization. The highly transformed internal structures of many of these zircons (thickened and blurred oscillatory zoning, and convoluted zoning) support this possibility (e.g., Hoskin and Black, 2000; Corfu et al., 2003). Accordingly, the scattered core ages from 400 to 322 Ma could be attributed to secondary Pb loss due to the disturbance of pre-Variscan zircons. Zircon rim ages allow the calculation of a weighted average age of 287.8 ± 3.6 Ma (Fig. 9A), which is an approximation to the age of the metamorphic granulitic peak.

7.2.5. Sample 99187 (SCS felsic granulite)

Ages determined in 32 zircon cores display a distribution characterised by a Permo–Carboniferous population (278–399 Ma) and scattered ages up to the Mesoproterozoic, which shows two intermediate Neoproterozoic peaks at ~552 Ma and ~635 Ma (Fig. 9B, E). Rims and homogeneous zircon ages (n = 11) concentrate in the range 272–298 Ma (Fig. 9F) and allow the calculation of a weighted average age of 284.9 ± 3.5 Ma (Fig. 9B). This can be considered the age of the granulitic peak and the Permo–Carboniferous population of zircon cores, most of them showing different secondary textures (Fig. 7), would likely result from Pb loss in an open system. Taking into account the relative abundance of pre-Carboniferous core ages, the most probable protolith would be a Neoproterozoic rock, either magmatic or sedimentary.

7.2.6. Sample 77746 (SCS pelitic granulite)

All U–Pb zircon ages (n = 63) of this sample are concentrated in the range 246–334 Ma (Fig. 9C, E). The zircon CL images show either a homogeneous (Fig. 7) or a core-rim structure and display similar textures to other SCS granulites (e.g., occasional oscillatory zoning, secondary textures, bright or dark homogeneous zircons). The geochronological data indicate that the high-grade metamorphic recrystallization of this metasediment has obliterated all vestiges of pre-Variscan ages. The calculated weighted average age is 277.3 ± 1.9 Ma (Fig. 9C), once excluded ages younger than that of the host mafic dyke.

7.2.7. Sample 77750 (SCS pelitic granulite)

Ages from zircon cores (n = 33) are mainly concentrated in the broad range of 242–380 Ma, with the only exception of two younger ages (215 Ma and 222 Ma) and a group of ages (10) scattered from Devonian to Neoproterozoic (Fig. 9D, E). Dark homogeneous zircon grains are more abundant, and their analyses (n = 31) overlap the above range towards its younger values (mostly from 241 Ma to 308 Ma). A weighted average age of 288.6 ± 4 Ma has been calculated for the latter zircons (Fig. 9D) (excluding data younger than the age of the host dyke). The above results imply that zircon cores are highly affected by the Variscan recrystallization and the U–Pb system re-equilibrated during granulite metamorphism.

8. Lu–Hf isotopes

A selection of zircons from each sample was analysed by LA-ICP-MS to get the Lu–Hf isotopic composition, resulting in 218 data points (200 if discordant zircons are excluded) (Supplementary Data, Table S5). These analyses were performed in the same spots selected for the U–Pb geochronology. The initial $^{176}Hf/^{177}Hf$ ratios has been determined using the age of the corresponding zircon core (for inheritances), the calculated magmatic age (for zircons clearly associated to a specific igneous event), or the calculated age of metamorphism (for rims and homogeneous zircons).

The initial $^{176}Hf/^{177}Hf$ isotopic ratios of metamorphic rims and rounded homogenous zircons from all samples are generally clustered in relatively narrow ranges (0.282116–0.282558 if all samples are considered), corresponding to subchondritic values (ε_{Hf} from –1.7 to –17.2; Fig. 10A). The only exception to this homogeneity is one analysis from sample 117455, which is much less radiogenic (ε_{Hf} = –37) than other metamorphic zircons from the same sample (Fig. 10A). Despite their overall similarity, Hf isotopes are slightly more radiogenic in metamorphic zircons from the Calatrava metagranitoid sample (117450) and the SCS felsic granulites (U50 and 99187) than the rest of samples. Only one SCS felsic granulite xenolith has provided Variscan zircons with positive ε_{Hf} values (up to + 4.1 at 297 Ma) (sample U-145 studied by Villaseca

Fig. 8. SHRIMP U–Pb data for zircons from the Calatrava granulite xenoliths. (A1, A2, A3) Concordia diagram and zircon age extractor results for sample 117449; (B) concordia diagram for sample 117455; (C1, C2, C3) concordia diagram, zircon age extractor and weighted average age for sample 117450. Error ellipses are given at the 2σ level. Blue bars represent rejected data; (D, E) probability plots of U–Pb zircon ages. (E) shows the distribution of ages in the range ~250–350 Ma, where the main peaks are related to metamorphic zircons and the Variscan magmatic zircons from samples 117449 and 117450. (For interpretation of the references to colour in this figure legend, the reader is referred to the web version of this article.)

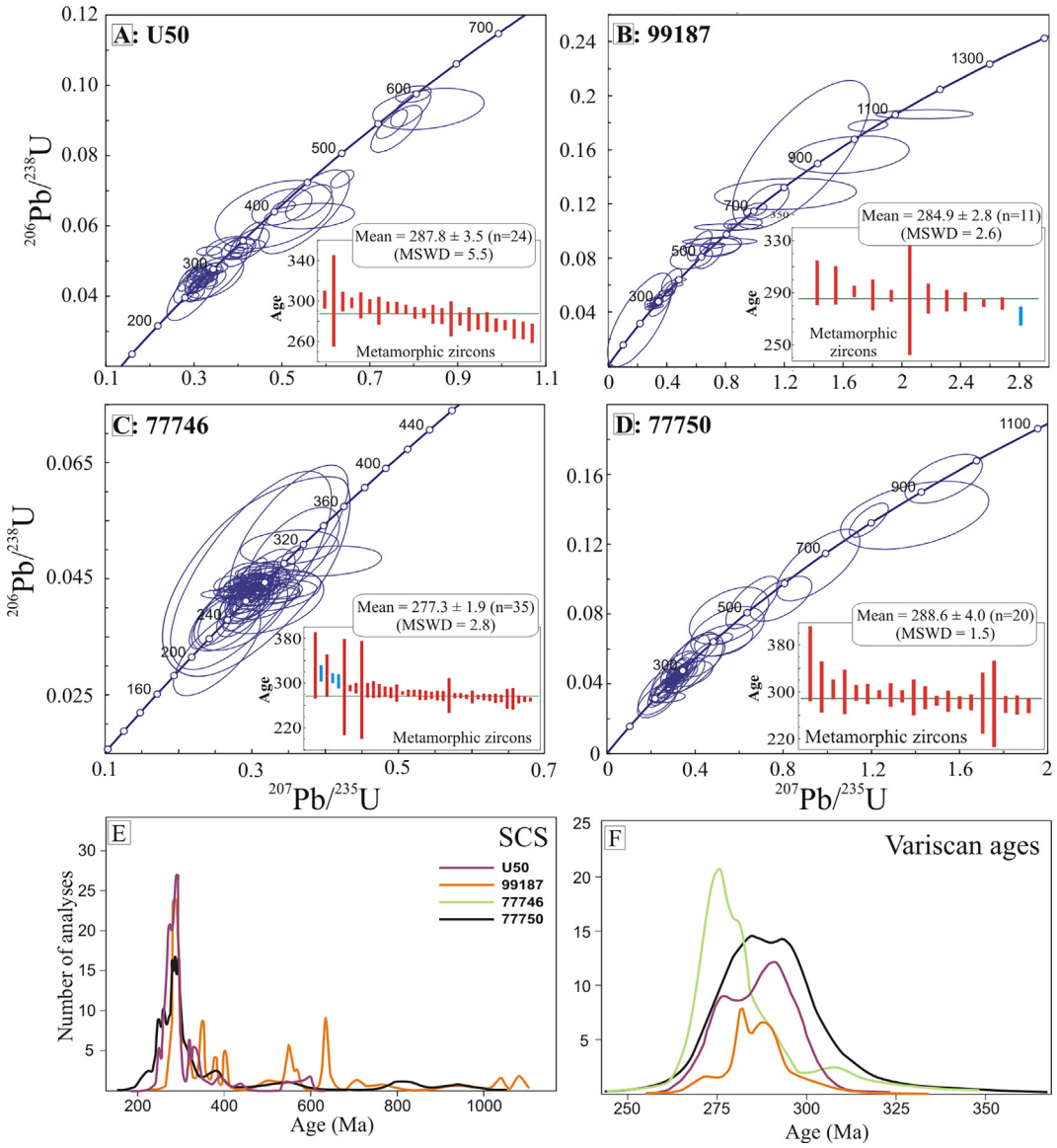

Fig. 9. SHRIMP U–Pb data for zircons from the SCS granulite xenoliths. Concordia diagrams and weighted average ages obtained for metamorphic zircons (insets) of samples U50 (A), 99187 (B), 77746 (C) and 77750 (D). Error ellipses are given at the 2σ level. Blue bars represent rejected data. (E, F) Probability plots of U–Pb zircon ages. (F) shows the distribution of ages in the range ~250–350 Ma, where the main peaks are related to metamorphic granulitic zircons. (For interpretation of the references to colour in this figure legend, the reader is referred to the web version of this article.)

et al., 2011). The analysed metamorphic zircons have low ^{176}Lu/^{177}Hf isotopic ratios (mostly < 0.0001). Analyses from zircon cores younger than ~450–500 Ma, which are likely affected by a secondary U–Pb age rejuvenation (recrystallization), show Lu–Hf isotopic ratios overlapping those of metamorphic zircons (Fig. 10B, C).

Inherited cores can broadly be divided into two groups: Cambrian–Neoproterozoic and Paleoproterozoic, with a clear Mesoproterozoic gap. The former population includes a more abundant zircon population and is characterised by initial Hf isotope ratios mostly in the range 0.281954–0.282629, representing a continuous composition from enriched to relatively depleted isotopic values (ε_{Hf} from −19.5 to + 11.5; Fig. 10B, C). Only four analyses fall outside this range, two of them displaying ε_{Hf} = −46 and two analyses with unrealistic highly radiogenic ε_{Hf} (+26.4 and + 27.4) values, which have not been plotted or considered in the discussion; it is likely that the Lu–Hf analysis drilled into a different domain than from where the U–Pb age was obtained. On the other hand, the Paleoproterozoic and Archean zircon cores (mostly from sample 117455) always display subchondritic values (^{176}Hf/^{177}Hf = 0.280 899–0.281911; ε_{Hf} from −2.0 to −19.5; Fig. 10B, C). ^{176}Lu/^{177}Hf ratios in all zircon cores display fairly heterogeneous values (0.000005–0.0026), but they are mostly above 0.0001.

9. Geothermobarometry

Pressure and temperature metamorphic peak conditions of the Calatrava and SCS xenoliths have been estimated on the basis of mineral equilibria. A more detailed study of the geothermobarometry of the SCS granulitic xenoliths can be found in previous works (Villaseca et al., 1999, 2007b; Orejana et al., 2011) and they will be considered here for comparison. However, we have taken into consideration the new dataset of zircon trace element contents (Ti) to estimate the temperature of the four SCS xenoliths included in the present study.

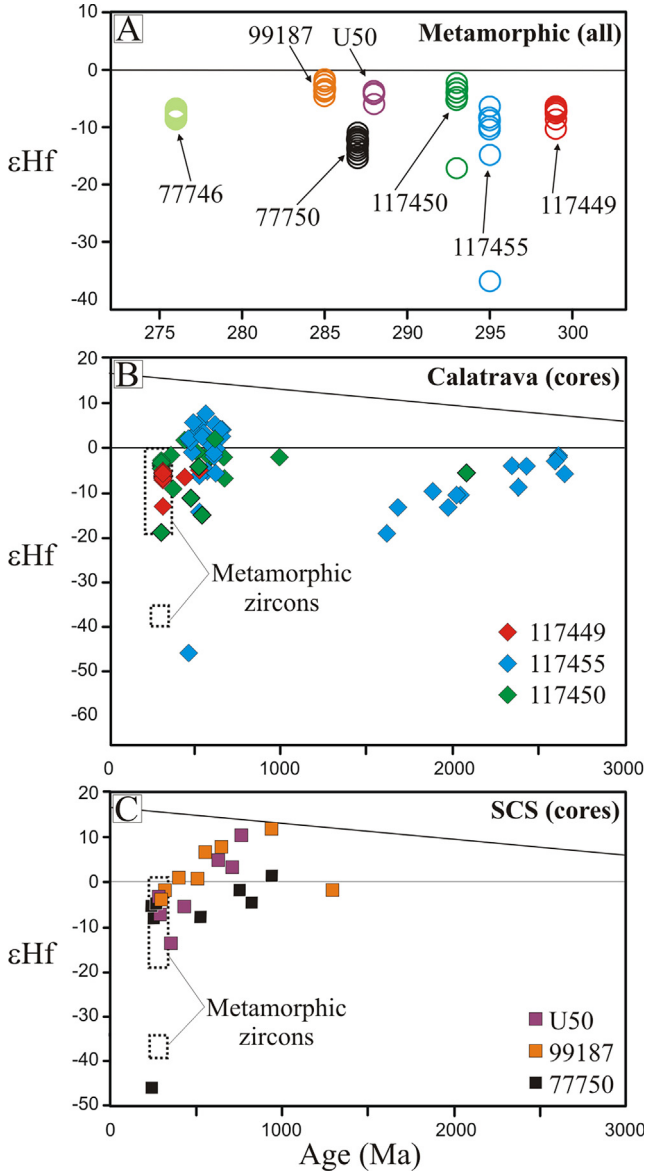

Fig. 10. Hf isotope composition of zircons from the SCS and Calatrava granulite xenoliths. (A) Metamorphic zircons (rims and homogeneous zircon grains) from both the SCS and the CVF areas; (B) zircon cores from Calatrava samples; (C) zircon cores from SCS samples. All symbols have a size which include the analytical error (±1σ).

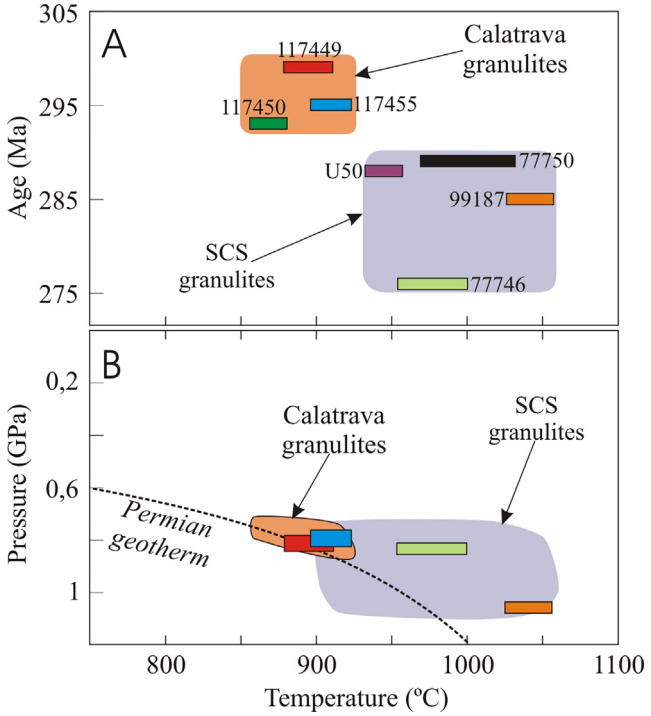

Fig. 11. Average pressure and temperature estimations obtained for the SCS and Calatrava granulite xenoliths. Each colour bar in (A) indicates the age and average temperature calculated in this study. Pressures estimations shown in (B) for samples 117449, 117455, 77746 and 99187 have been estimated with classic geobarometers and the software of Reche and Martínez (1996) (see more detail in Supplementary Data, Table S6). The field of SCS granulites in (B) is after Villaseca et al. (1999, 2007b). The Permian geotherm has been taken from Villaseca et al. (2005).

Temperature has been calculated using the recalibrated Ti-in-zircon and Zr-in-rutile thermometers (Ferry and Watson, 2007). A value of a_{SiO_2} = 1 and a_{TiO_2} = 1 has been used in the calculation when quartz and rutile are present in the rock, otherwise, the activity has been kept at a value of 0.7, according to the recommendations given by Ferry and Watson (2007). The average Ti-in-zircon temperatures obtained (Supplementary Data, Table S6A) are consistent with a high-T (HT) metamorphic event at granulite facies conditions for the Calatrava samples, and ultra-high-T (UHT) metamorphic conditions (>920 °C) for the SCS samples, as previously stablished (e.g., Orejana et al., 2011). The lack of zoning in mafic mineral (such as garnet) is in accordance with a high-temperature recrystallization. The three samples from Calatrava provide average temperatures in the range 869–910 °C, whereas the SCS samples show higher values (944–1041 °C) (Fig. 11A). This latter temperature range overlaps the results obtained for other SCS granulite xenoliths using the same thermometer (Orejana et al., 2011), but are slightly higher than temperature estimates based on more classic thermometers for other SCS granulite xenoliths (e.g., grt-bt and grt-opx pairs; Villaseca et al., 1999). The Zr-in-rutile thermometer of Ferry and Watson (2007) could only be used for one CVF garnet felsic granulite (117455) (Supplementary Data, Table S2E) and the average temperature estimated (T = 842 °C) is lower than its correlative obtained using the Ti-in-zircon method (T = 910 °C).

Pressure has been estimated using classic mineral equilibria formulas as a function of the mineral assemblage present in the analysed xenoliths. The GPT worksheet of Reche and Martínez (1996), which implements calculations based on a large set of such barometers, has been used (Supplementary Data, Table S6B). Average pressures of 0.82, 0.79 and 0.76 GPa have been obtained for the Calatrava type-II metasedimentary granulites (samples 117453, 117454 and 117455, respectively) using different formulas for the GASP (grt-sill-pl-qtz) barometer, and an average pressure of 0.84 GPa was obtained for sample 117449 applying grt-opx-pl barometers (see references in Supplementary Data, Table S6). Only two SCS xenoliths allowed calculations of pressure estimates, providing averaged pressures of 1.11 (sample 99187) and 0.82 GPa (sample 77746). An input temperature of 900 and 1000 °C has been used for the Calatrava and SCS xenoliths, respectively, when needed. These results would indicate similar equilibration depths for the Calatrava metasedimentary granulites when compared to the charnockitic xenoliths (Fig. 11B), overall in the range of ~25–27 km, corresponding to the current CVF lower crust.

A few xenoliths did not provide temperature and/or pressure estimates because they were not selected for a detailed zircon chemical study, due to lack of a suitable mineral assemblage or owing to total transformation of garnet to kelyphites. Nevertheless,

the petrographic homogeneity shown by the metagranitoid xenoliths point to similar *P-T* conditions for samples 117448, 117450 and 117452. On the other hand, the same extrapolation is not possible for the charnockitic granulites. The absence of garnet in charnockite 117451, together with the recognition of gneissic foliation and the presence of up to 8% biotite, probably means that this charnockitic xenolith equilibrated at lower *P-T* conditions when compared to the garnet-bearing 117449 type-I granulite. Minor differences in the mineral chemistry of orthopyroxene from these xenoliths (Supplementary Data, Fig. S2) could also be explained by the different mineral paragenesis, such as the higher Al contents in sample 117449, likely associated to growth in equilibrium with metamorphic garnet. Accordingly, the xenolith suite from the La Encomienda volcano seems to represent a sampling of the deep crust at different levels. The variable modal abundance of biotite in the studied xenoliths might also be an effect of such different *P-T* conditions, as the higher-*T* xenoliths are depleted in biotite probably as a result of the ongoing biotite dehydration-melting reaction (850–930 °C; Patiño Douce and Beard, 1995). The lack of reliable pressure estimations for charnockite 117451 and the metagranitoid xenoliths do not allow assigning a precise depth for these rocks. Taking into account that the temperatures recorded in zircons from metagranitoid 117450 are only slightly lower than the rest of Calatrava xenoliths, and the moderate slope of the geotherm estimated for central Spain during Permian (Villaseca et al., 2005), no big differences should be expected in their level of extraction, as represented in Fig. 11B.

The average temperatures recorded in the SCS granulites (~900–1050 °C; Orejana et al., 2011 and this study), as well as the pressures obtained in samples 77746–99187 and those previously estimated in similar xenoliths (mostly in the range of 0.9 to 1.1 GPa; Villaseca et al., 1999, 2007b), are slightly higher than those of the Calatrava xenoliths (Fig. 11). These data are in accordance with the almost complete dehydration of biotite, the restitic nature of these xenoliths (Villaseca et al., 1999) and the formation of abundant rounded zircons with a variety of zoning patterns (Orejana et al., 2011), typical of high-grade metamorphic zircons formed by dissolution–reprecipitation in an anatectic environment (Nemchin et al., 2001). Other mineral features of the SCS felsic granulites characteristic of UHT granulitization are: (i) the presence of accessory residual Ti-rich phlogopite (absence of biotite), (ii) the high LREE contents of feldspars and high orthoclase of plagioclase (antiphertite varieties), (iii) the presence of Zr-rich garnet and Zr-rich rutile (as the main Ti-bearing phase), (iv) the common occurrence of orthopyroxene and (v) the absence of kyanite. These features, which differ from those of the Calatrava xenoliths, support a slightly deeper crustal level of extraction and higher metamorphic grade for the SCS xenoliths when compared to the Calatrava suite, although some overlap in the pressure of equilibration (at about 0.8 GPa) is possible (Fig. 11B).

10. Discussion

10.1. Variscan magmatic rocks in the Calatrava lower crust

The new suite of granulite xenoliths sampled in the La Encomienda volcano (Calatrava Volcanic Field) is representative of a heterogeneous lower crust, and includes metagranitic, charnockitic and garnet-sillimanite-bearing metasedimentary types.

The two former groups can be related to Variscan metaigneous protoliths. This conclusion is supported by the U–Pb zircon geochronology, as all zircon crystals from samples 117449 and 117450 are elongated prisms with large inner areas showing oscillatory zoning (Fig. 7) and ages mostly restricted to a narrow Variscan range (Fig. 8A1, C1). These characteristics are typical of a magmatic zircon population and both samples only display occasional older inherited cores (Table 1). Nonetheless, the nature of the magmatic protolith is different in each case. The modal composition of metagranitic xenoliths is dominated by An-poor plagioclase, K-feldspar and quartz (summing up to 85–95 vol.%, Table 1), with minor mafic minerals (biotite < 7%), proportions which make them akin to felsic rocks such as granitoids. The absence of Al-rich granulitic minerals (e.g., garnet, sillimanite) and the recognition of magmatic textures in these rocks imply that metamorphism is manifested mainly by moderate recrystallization.

The two charnockitic xenoliths display a similar whole-rock major element composition, equivalent to that of leucodiorites. Sample 117451 is more primitive (Mg# = 0.69) than sample 117449 (Mg# = 0.61), which is also apparent in the more anorthitic plagioclase (Supplementary Data, Fig. S1A) and higher Mg# in orthopyroxene (Supplementary Data, Fig. S2A). Moreover, they have contrasting trace element contents and modal mineralogy. Sample 117449 exhibits Th, Zr and LREE abundances much higher than sample 117451 (Fig. 5), and even higher than those of highly evolved magmatic rocks (such as granites). This unusual composition might be associated to a high modal abundance of accessory phases with very high concentrations of the above elements (e.g., zircon, monazite) and cannot be considered representative of a possible magma composition. Sample 117451 displays a pattern representing much lower abundances for most trace elements, and slight positive peaks at Eu and Sr which point to some degree of plagioclase accumulation (Fig. 5).

The geochronological U–Pb zircon data indicate magmatic crystallization ages related to the Variscan cycle: 314 Ma for the charnockitic granulites (sample 117449) and 308 Ma for the metagranitoids (sample 117450) (Fig. 8A3, *C2*). These ages are similar to those determined for nearby felsic batholiths formed in the context of the Variscan continental collision (316–285 Ma; Carracedo et al., 2009; Orejana et al., 2012, 2020; Merino–Martínez et al., 2014; Errandonea et al., 2017). Considering that the above felsic magmatism is late to post-tectonic, the protoliths of types I and III Calatrava xenoliths likely represent intermediate–felsic magmas that stagnated and crystallized in the lower crust and that were coeval with the magmatic Variscan rocks that intruded into shallower crustal levels.

The composition of the two analysed metagranites (117448 and 117450) fits that of outcropping evolved granites from central Spain (Fig. 4). Likewise, the composition of the charnockitic granulites (117449 and 117451) plot towards the gabbro-diorite compositional pole of the Variscan magmatism. Metagranites and charnockitic granulites from Calatrava share similar Sr–Nd isotopic ratios (Fig. 6), which might point to some kind of genetic relationship, and the Hf isotopic signatures of their Variscan magmatic zircons are coherent with the Nd isotopic values (ε_{Hf} mostly from –1.7 to –6.9; Fig. 10B). A common origin by crystal fractionation is possible, but the scarce number of xenoliths available and the lack of metaigneous xenoliths with an intermediate composition between the metagranitic and charnockitic poles, do not allow decisive conclusions to be drawn. The Nd isotopic ratios of these SiO_2-rich metagranites are more radiogenic (closer to the Bulk Silicate Earth) than most central Spain granitoid series (Fig. 6) and compatible with magmas derived from an enriched mafic–intermediate crust. Mantle-derived magmas are volumetrically scarce in the Variscan Iberian realm (e.g., Orejana et al., 2009; Scarrow et al., 2009), as are mafic granulites in the Iberian lower crust (Villaseca et al., 1999, 2007b). Moreover, the highly felsic nature of the Calatrava metagranitoid xenoliths and their peraluminous composition make unlikely an origin by differentiation from mafic magmas. Accordingly, a more plausible scenario would require melting of intermediate to felsic crustal rocks (either of igneous or sedimen-

tary origin), which might yield a primary magma with a composition from leucotonalite to granite (e.g., Skjerlie and Johnston, 1996; Springer and Seck, 1997; Sisson et al., 2005) and would require much less or no subsequent fractionation.

The magmatic age and isotopic ratios of the metaigneous Calatrava types I and III xenoliths are very similar to those of the Los Pedroches and NW Iberia I-type granites (see Fig. 6 and references in its caption). Considering this similarity, these granulite xenoliths might be the high pressure equivalents of upper crust Variscan magmatic intrusions, which underwent granulite-facies metamorphism at the lower crust. Their juvenile isotopic composition (close to BSE values) is in accordance with sources related to the accretion or emplacement of basic to intermediate rocks within a mainly metasedimentary crust during the closure of oceanic basins, prior to the Variscan continental collision. Such processes would have taken place at the boundaries between the Central Iberian Zone and neighbouring terranes: Galicia Tras-Os-Montes and Ossa-Morena Zones (e.g., Simancas et al., 2002; Arenas et al., 2007). Iberian I-type granite plutons far from such marginal areas (mostly those from the SCS), which exhibit less radiogenic Nd values, have been explained as derived from more enriched crustal sources, leaving a residue that might be similar to the metaigneous SCS felsic granulites (Villaseca et al., 2009). The higher silica content of the Calatrava metagranitoid xenoliths supports melting of a highly felsic source rock. This source could be of sedimentary origin, as deduced from the scattering of pre-Variscan ages shown by zircon cores from sample 117450, mainly concentrated in the Neoproterozoic (Fig. 8D). Taking into account the above geological setting, arc-related mafic rocks and volcanoclastic sediments are likely sources for the generation of intermediate–felsic magmas with relatively high ε_{Nd} values.

10.2. Metasedimentary protolith of the Calatrava garnet felsic granulites

The garnet felsic granulites, represented by sample 117455, display a silica-rich (SiO_2 = ~65 wt.%) and moderately peraluminous (ACNK = 1.3) composition (Table 2). The scarcity of aluminous minerals such as sillimanite or kyanite argue against a metapelitic s.s. nature. Moreover, this sample plots far from the field of the SCS metapelitic lower crustal xenoliths, which are more peraluminous and mafic and less sodic. Rather, this sample falls within the field of the SCS felsic granulites (Fig. 4). This latter group of xenoliths has been associated to Neoproterozoic–Early Ordovician felsic metaigneous protoliths (Villaseca et al., 1999, 2011). The U–Pb ages recorded in zircons from sample 117455 show a distribution characterised by multiple populations, with a main group of Neoproterozoic ages (Fig. 8D). Another cluster could be assigned to the Variscan cycle (~270–360 Ma) and the rest of data yield several minor peaks from Paleoproterozoic to Neoarchean. These latter zircon cores are underestimated in Fig. 8D, because many of them are discordant and have therefore not been included in the probability density diagram. However, the $^{207}Pb/^{206}Pb$ ages of these discordant zircons are too high to be representative of Neoproterozoic or younger data and are likely older than ~1600 Ma. Although not considered for any discussion requiring precise geochronological data, these zircons can be added to the rest of old zircons from this sample to estimate the relative abundance of cores with Paleoproterozoic–Neoarchean ages (reaching up to ~37%). The relative abundance of such old ages, together with the scatter of the Neoproterozoic population and the absence of zircon grains showing old (pre-Neoproterozoic) inheritances inside Neoproterozoic mantles, would favour that the protolith is a Neoproterozoic non-pelitic (metapsammite) sediment, rather than a Neoproterozoic felsic igneous rock. Chemical classification diagrams for sediments (Pettijohn et al., 1972) point to graywackes–arkoses as the most likely candidate.

The radiogenic Nd value of sample 117455 (ε_{Nd} = –8) falls within the range provided by low-grade Neoproterozoic–Cambrian metasedimentary rocks outcropping in southern CIZ (–4.4 to –9.5 when back-calculated to 309 Ma; Ugidos et al., 2003; López-Guijarro et al., 2008; Villaseca et al., 2014), known as the Schist–Greywacke Complex (SGC). The geochronology and Hf isotope ratios of zircons from the SGC (Orejana et al., 2015) and the analysed metasedimentary granulite also provide significant similarities, namely the presence of the same pre-Variscan age populations (Neoarchean, Paleoproterozoic, Tonian and Ediacaran–Cryogenian) and the predominance of Neoproterozoic zircons showing heterogeneous Hf isotope ratios (moderately positive to slightly negative ε_{Hf} values; Fig. 10B). On the other hand, whole-rock chemical differences exist with respect to the Schist Greywacke Complex (SGC) metasediments: sample 117455 displays higher Ca, Si, Sr, Zr, Ce, and lower Al, Rb and Th when compared to the Neoproterozoic Iberian Average Shale (NIBAS), representative of the average composition of the metapelitic SGC (Fig. 4). The above data supports the possibility that the studied garnet felsic granulites represent fragments of deep-seated Neoproterozoic metasediments formed in a similar geodynamic setting as the SGC, although not totally equivalent to the observed shallow-level sequences. The high modal abundance of Al-rich minerals in the aluminous granulites described by Puelles et al. (2019) likely indicates that they also correspond to a metasedimentary protolith of a more pelitic composition.

10.3. Granulite-facies metamorphism in central Iberia

Zircons from all the studied xenoliths display textural features typical of high-grade metamorphic conditions: growth of dark rounded crystals (either unzoned or with sector zoning), regrowth of rims around inherited grains and secondary textures such as convoluted zoning, widening of bands or highly luminescent areas (Fig. 7) (e.g., Corfu et al., 2003). Temperatures calculated with the Ti content of these zircons are compatible with equilibration at high-*T* granulite-facies conditions (~870–1040 °C). The mainly flat HREE chondrite-normalised patterns and low Lu/Hf ratios and Y concentrations of these zircons (Fig. 3) agree with formation in equilibrium with garnet (e.g., Schaltegger et al., 1999; Whitehouse and Platt, 2003). The high Nb and Ta contents of oscillatory zoned inherited zircon cores (Fig. 3D) are typical of a magmatic origin (e.g., Belousova et al., 2002). Nevertheless, some granulitic zircons mimic the composition of igneous crystals (Fig. 3) and display variable HREE patterns within a single sample (e.g., 117449, Supplementary Data, Table S3), the latter feature being also present in garnet from sample 117455 (Supplementary Data, Fig. S3B). This kind of chemical variability, which has already been described in the SCS felsic granulites (Orejana et al., 2011), is likely related to Rayleigh fractionation of strongly compatible but slowly diffusing elements (Y, REE) during garnet growth in the presence of melt (Otamendi et al., 2002). The above data, as well as the calculated high temperatures and petrographic features (e.g., biotite scarcity), point to zircon growth in an anatectic environment beneath Calatrava and the SCS, and reinforces the idea of a general restitic nature for the central Iberia lower crust. The slightly elevated LREE contents of K-feldspar and plagioclase from the CVF types I and II xenoliths (Supplementary Data, Fig. S1C), which are close to those from feldspar in the SCS granulites, also support the possibility that feldspar in restitic granulite-facies rocks can be an important phase controlling the behaviour of such trace elements (Villaseca et al., 2007a).

U–Pb ages of metamorphic zircons are different for each region (Figs. 8 and 9): older for Calatrava (~292–299 Ma) and younger for

the SCS (~277–289 Ma). In the case of the SCS, there is a clear overlapping of the calculated ages within a narrow range (284–289 Ma) for xenoliths U50, 99187 and 77750, whereas granulite 77746 have provided the youngest age (277.3 Ma). Apart from these differences, the SCS xenoliths also show slightly higher equilibrium pressures and temperatures (Fig. 11). The apparent relationship between age and *P-T* conditions could imply also that attainment of metamorphic high-T peak conditions was diachronic, progressing from slightly shallower (Calatrava) to deeper levels (SCS), which fits the results from thickening models in collisional orogens (e.g., Spear, 1993). However, the association of specific ages to HT or UHT metamorphic events ($T > \sim 900$ °C) is challenged by: (1) the long-lasting timespan (several tens of Ma) they may register (e.g., Rubatto et al., 2001), and (2) the disturbance and reequilibration of the zircon U–Pb isotopic system at temperatures above 850 °C (Kunz et al., 2018). The latter authors point out that the younger ages shown by granulite-facies rocks, when compared to amphibolite-facies rocks affected by the same metamorphic event, is likely related to elemental diffusion (e.g., Pb) in the zircon crystal lattice, possibly causing partial resetting of the U–Pb ages (e.g., Cherniak and Watson, 2003; Hoskin and Schaltegger, 2003). The UHT conditions reached by the SCS granulite xenoliths might explain their younger age peaks and lower amount of inherited zircons (and higher neoformed zircon grains), when compared to the Calatrava granulites. Taking into account that granulite-facies metamorphism can last for >30 Ma (e.g., Rubatto et al., 2001), constraining its age would require an extensive database rather than peak or average calculated ages only. Thus, we have plotted together the available zircon U–Pb ages of samples from central Spain to obtain a more precise distribution of these metamorphic ages (Fig. 12). It follows that: (1) no significant differences exist in the distribution of ages for the SCS granulites, either considering only data from our study or the whole dataset, (2) the distribution of ages for the Calatrava samples is broadly coincident with that of the SCS granulites, and (3) the main range of ages (considering both the largest primary and secondary peaks) is broadly restricted to 275–299 Ma (mostly in the range of 285–299 Ma). We can infer from these data that the granulite-facies metamorphism is roughly coeval in the SCS and the Calatrava lower crust, although the youngest zircons (up to 277 Ma in sample 77746) are only found in the SCS granulites. Thus, the younger ages in this SCS sample are likely related to a long-lasting reequilibration of the zircon isotopic system due to their UHT conditions.

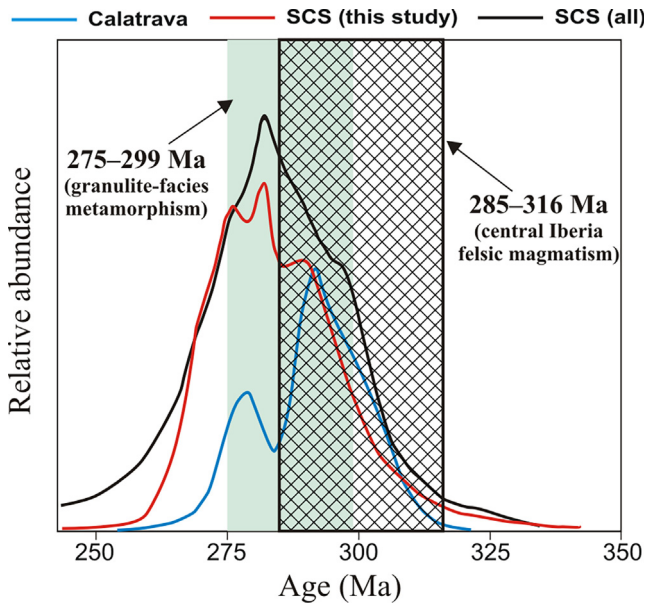

Fig. 12. Probability density curves of metamorphic zircon ages of the SCS and Calatrava granulite xenoliths. SCS (all) ages consider those from this study as well as data from Fernández-Suárez et al. (2006) and Orejana et al. (2011). The age range of 275–300 Ma has been bracketed taking into account the largest primary and secondary peaks of the three density curves. The range of 285–316 Ma for the central Spain felsic magmatism considers data from Carracedo et al. (2009), Orejana et al. (2012, 2020), Merino–Martínez et al. (2014), Errandonea et al. (2017), and references therein.

This reequilibration might also explain the age difference between the Variscan granulite-facies metamorphism and the outcropping granite intrusions in central Iberia. A genetic relationship has already been proposed indicating that the granulite xenoliths might represent the restitic counterpart after the extraction of felsic magmas (Villaseca et al., 1999; Fernández-Suárez et al., 2006; Orejana et al., 2011). The available zircon geochronology highlights that granulite ages overlap the granite ages, but with some displacement towards younger values (Fig. 12). Such mismatch could in part be explained by the long-term resetting of the U–Pb isotopic system in zircon from HT and UHT granulite-facies conditions at lower crustal levels. In such cases, ages in granulite-facies rocks would preferentially represent the transit from high-*T* peak conditions to attainment of the zircon U–Pb closure temperature (the post-peak cooling history of the rock). The experimental work of Tomkins et al. (2007) for high-grade rocks with quartz and rutile has also related zircon growth to the retrograde path, as zircon tends to be resorbed during prograde metamorphism. The scarcity (or absence) of zircon ages matching the older part of the age range representative of the central Iberia felsic magmatism (~285–316 Ma) implies that zircon formed during the first stages of melting hardly resisted the protracted history of high-T conditions associated to the late orogenic stages and the long period of thermal recovery after crustal thickening (the post-metamorphic peak conditions evolved from circa 900 °C at 285 Ma to the current 700 °C estimated at Moho depths beneath the SCS; Jiménez-Díaz et al., 2012).

All granulitic zircons display subchondritic Hf isotope ratios (ε_{Hf} mostly from –1.7 to –17.2; Fig. 10A), in accordance with the context of crustal recycling during the Variscan continental collision. Growth of new zircon during granulite-facies conditions is usually associated with recrystallization and local dissolution-reprecipitation, either in the solid state or during anatexis (Hoskin and Schaltegger, 2003), but the Lu–Hf isotopic ratios may remain unaffected (e.g., Amelin et al., 2000) and follow an evolution dictated by a low $^{176}Lu/^{177}Hf$ ratio of ~0.001 (typical of zircon). Thus, the main control exerted by zircon on Hf behaviour implies that the above isotopic composition may reflect that of pre-existing zircons (protolith) at the time of metamorphism. The strong similarity between $^{176}Hf/^{177}Hf$ ratios of the abundant Neoproterozoic (SCS) or Variscan (Calatrava) zircon cores of all samples and those shown by the metamorphic zircons (Fig. 13A) supports the above possibility and precludes an important role for other phases in controlling the Hf budget, such as garnet, whose breakdown can release highly radiogenic Hf (Slama et al., 2007). Disturbance of the U–Pb isotopic system during high-T metamorphism can also explain the presence of zircon cores with concordant pre-Variscan and post-Cadomian ages in a time span (~350–480 Ma) devoid of relevant felsic magmatism in central Iberia.

10.4. Inferences on the evolution of the lower crust under central Spain

The age distribution obtained from zircon cores (Figs. 8D and 9E) indicates that the studied granulites represent either magmas extracted from Early Paleozoic–Neoproterozoic crustal materials or sediments deposited in this time period. This is in accordance with the geodynamic context of the Central Iberian Zone during

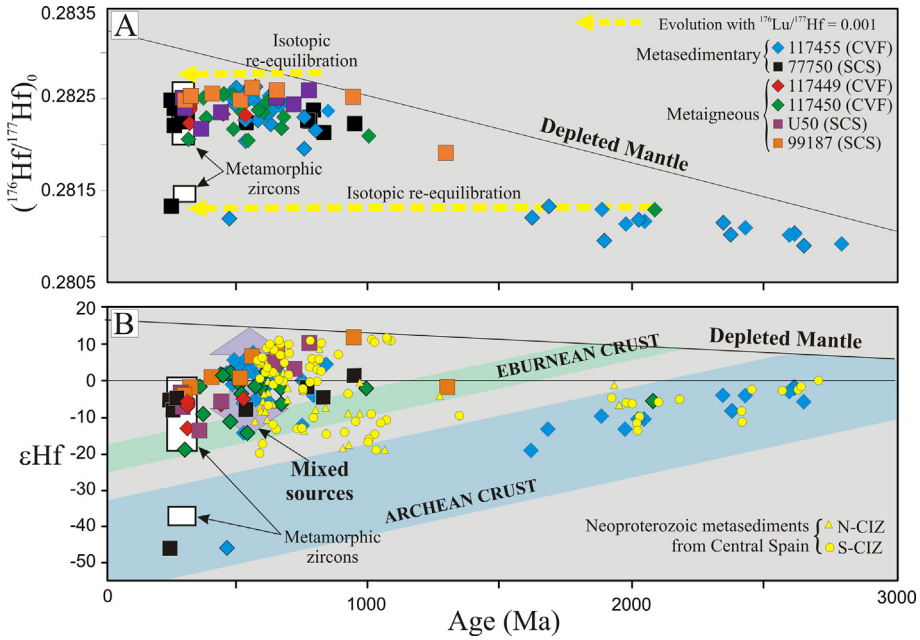

Fig. 13. Initial $^{176}Hf/^{177}Hf$ (A) and ε_{Hf} (B) evolution diagrams summarising the data of zircon from the analysed SCS and Calatrava granulite xenoliths. The composition of metamorphic zircons is represented with white rectangles. The composition of detrital zircons from the northern and southern Central Iberian Zone Neoproterozoic metasediments (N-CIZ and S-CIZ, respectively) have been taken from Orejana et al. (2015). Two colour bands representing the Hf isotope evolution of two juvenile crust components of Eburnean (1800–2200 Ma) and Archean (~2500–4000 Ma) age are shown, considering a $^{176}Lu/^{177}Hf$ ratio of 0.012. The broad yellow dashed arrows represent the evolution path of zircons which might have been affected by isotopic re-equilibrium due to the granulite-facies metamorphism, following a $^{176}Lu/^{177}Hf$ ratio of 0.001, typical of zircon. (For interpretation of the references to colour in this figure legend, the reader is referred to the web version of this article.)

the Late Neoproterozoic, which was located close to the continental arc system (Cadomian orogeny) of the northern margin of Gondwana (e.g., Orejana et al., 2015 and references therein). The prevalence of Neoproterozoic zircon populations in Early Paleozoic igneous and sedimentary rocks from central Spain reflects the direct influence of the Cadomian magmatism and back-arc sedimentation in their sources (e.g., Talavera et al., 2012, 2013; Fernández-Suárez et al., 2014; Orejana et al., 2015). Accordingly, zircon data from the studied granulite xenoliths also shows the influence of this subduction magmatism and suggests that the lower crust under central Spain is mainly constituted by arc-related metaigneous or metasedimentary rocks.

Constraining the precise ages of these protoliths is not straightforward. The metasedimentary granulite 117455, from the CVF, is characterised by the abundance of Neoproterozoic ages (~530–700 Ma), the well-preserved magmatic textures of these zircons (typical oscillatory zoning) and the sedimentary origin of the protolith. These features support a Neoproterozoic maximum depositional age in the range 530–560 Ma, corresponding to the extent of the maximum peak of the probability density curve (Fig. 8D). Zircons from this sample also include a relatively high number of Cambrian–Ordovician ages, which are much less abundant in the rest of Calatrava granulite xenoliths (Supplementary Data, Table S4). The end of the Cadomian orogenic cycle in the Iberian Massif implies a complex geodynamic setting still under discussion which includes a protracted event of felsic magmatism, mostly from 496 to 481 Ma (e.g., Villaseca et al., 2016; García-Arias et al., 2018). However, zircons with Cambrian and Ordovician ages from these CVF granulites display textural features in accordance with U–Pb isotopic disequilibrium due to the Variscan high-T metamorphism and are unlikely to be related to the above Paleozoic felsic magmatism. These data suggest that the lower crust under this area is probably composed predominantly of Neoproterozoic metaigneous and metasedimentary rocks associated with the Cadomian continental arc setting. Studies of Variscan granites of south-central Spain, based on the U–Pb–Hf isotopic composition of inherited zircons, have proposed similar crustal sources for the felsic melts (Merino–Martínez et al., 2014). Nevertheless, other studies focused on further north granitic intrusions have highlighted the involvement of Early Paleozoic metaigneous sources, at least under the SCS (Orejana et al., 2012; Villaseca et al., 2012).

The Neoproterozoic zircons yield a wide range of Lu–Hf isotope ratios (ε_{Hf} from −19 to + 11.5), although they are mostly positive epsilon (Hf) values (Fig. 13B). The abundant juvenile signatures agree well with an active continental arc playing a relevant role in the genesis of the granulite sources, whereas the marked isotopic variability would be explained by mixture with an older and more evolved component (Fig. 13B). The interpretation of the latter component differs depending on the nature of the protolith considered. Epsilon (Hf) values for Neoproterozoic inherited zircons included in the metaigneous granulites from Calatrava and the SCS are all above −20 (Fig. 13B). This feature suggests that the Neoproterozoic crustal component which mixed with the juvenile magmas was likely derived from an Eburnean crust, rather than something older (Fig. 13B). The presence of an Eburnean crust has been identified in cratonic terranes located in northern Africa (e.g., Ennih and Liegeois, 2008) and in Neoproterozoic metasediments deposited in nearby basins (e.g., Avigad et al., 2012), relatively close to the position proposed for the Central Iberian Zone during the Neoproterozoic (Orejana et al., 2015). Thus, the Neoproterozoic crust under this Cadomian realm might have been composed mainly by rocks extracted from, or related to, a juvenile Eburnean crust, not older than ~2200 Ma. On the other hand, zircons in granulites with a sedimentary protolith, such as sample 117455 from Calatrava, represent detritus resulting from the erosion of near or distant outcropping rocks. In this case, the abundant Neoproterozoic detrital zircons with predominantly positive ε_{Hf} values (Fig. 10B) are likely derived from the Cadomian continental arc, whereas the Paleoproterozoic and Archean zircon populations, with relatively evolved Hf isotope signatures, could come from old

cratonic terranes located in the Gondwana hinterland. The Hf isotope ratios of these latter zircons are in accordance with the evolution of an Archean crust, which has also been identified in outcropping Neoproterozoic metasediments from the CIZ (Orejana et al., 2015) (Fig. 13B). The few Variscan zircons with very low ε_{Hf} values (<−35), which are only present in metasedimentary granulites, also agree with such Archean component and are probably derived from Paleoproterozoic or Archean zircons which experienced the resetting of the U–Pb isotopic system during the high-grade metamorphism (Fig. 13A).

10.5. A heterogeneous lower crust under central–eastern Iberia

Lower crustal granulite xenoliths from the CIZ are found in post-Variscan alkaline mafic magmas of Permian to Cenozoic age from the Spanish Central System and the Calatrava Volcanic Field (Fig. 1). The granulites from the SCS are much more abundant and dispersed (Villaseca et al., 1999) than those recorded in the Calatrava volcanic field, which are restricted to a single volcano. From a statistical point of view, this makes the SCS granulites more reliable regarding estimations of the lower crust composition (Fig. 1). Several studies have stated that the lower crust under the SCS consists mainly of peraluminous felsic rocks, accompanied by minor metapelites and charnockites (and rare pyroxenites) (e.g., Villaseca et al., 1999, 2007b). The origin of these felsic and pelitic granulites has already been related to a combination of metaigneous and metasedimentary protoliths (Villaseca et al., 2011), whereas the charnockitic and pyroxenitic types would represent melting residues of intermediate composition and Variscan cumulates from mafic calc-alkaline magmas (Orejana et al., 2006; Villaseca et al., 2007b).

The granulite xenoliths described in the CVF are mostly quartz-rich felsic types: metagranitoids and garnet felsic granulites (Puelles et al., 2019; this work). Only the charnockitic xenoliths represent residual granulites with a more intermediate composition. The lower crust under the CVF resembles that below the SCS, considering the predominance of felsic lithologies and the absence or scarcity of true mafic xenoliths (Fig. 14). However, a significant difference between both areas is the occurrence of late Variscan metaigneous protoliths in the Calatrava granulites, which have not been identified in the SCS (Fig. 14). The metagranitoids and the intermediate leucodioritic granulites represent plutonic bodies crystallized in the mid-lower crust only a few million years before they reached the granulite-facies metamorphic peak, whereas the rest of granulites from the CVF seem to represent Neoproterozoic metasedimentary protoliths. On the other hand, the most abundant lower crustal xenoliths sampled in the SCS are felsic granulites mainly interpreted as Early Paleozoic metaigneous intrusions. These features indicate that the lower crust under central Spain is composed of Neoproterozoic metasediments and metaigneous intrusions, the latter representing older magmatic events under the SCS (Late Cadomian Cambrian–Ordovician magmatism) as opposed to the younger igneous event (Variscan) recorded beneath the southern CIZ (Calatrava).

Orthopyroxene-bearing xenoliths also appear in two Cenozoic alkaline volcanic regions from Eastern and South Eastern Iberia (Fig. 1). Nevertheless, they exhibit significant differences with respect to the SCS and CVF charnockitic xenoliths. They usually display a cumulus texture, although signs of metamorphic reequilibration may also be present (Eastern region). They also have a more mafic composition and are associated to mafic–ultramafic types, such as amphibole-phlogopite clinopyroxenites (Tallante volcano; Bianchini et al., 2015) or olivine-bearing metagabbros and clinopyroxenites (Cofrentes volcano; García-Rodríguez et al., 2022). Moreover, orthopyroxene from these *meta*-norites shows higher Cr and Mg# values, and these xenoliths have a metaluminous composition (Bianchini et al., 2013, 2015; and unpublished data). The age of some of these mafic cumulates is late Miocene (6.8 ± 2.0 Ma, U–Pb in zircon; Bianchini et al., 2015). This markedly younger age has not been recorded in any granulite xenolith suite entrained in Iberian alkaline magmas, apart from these volcanoes related to the Alpine and Betic-Rif orogenic belts (Fig. 1). There are significant differences in the nature and composition of crustal and lithospheric sections between the central Iberia Variscan terranes and the basement under the Cenozoic eastern Iberia Mountain ranges (Alpine orogenic processes s.l.) (Diaz et al., 2021) (Fig. 14). Further petrological and geochronological studies in the Cofrentes *meta*-noritic xenoliths have to be undertaken to clarify this model.

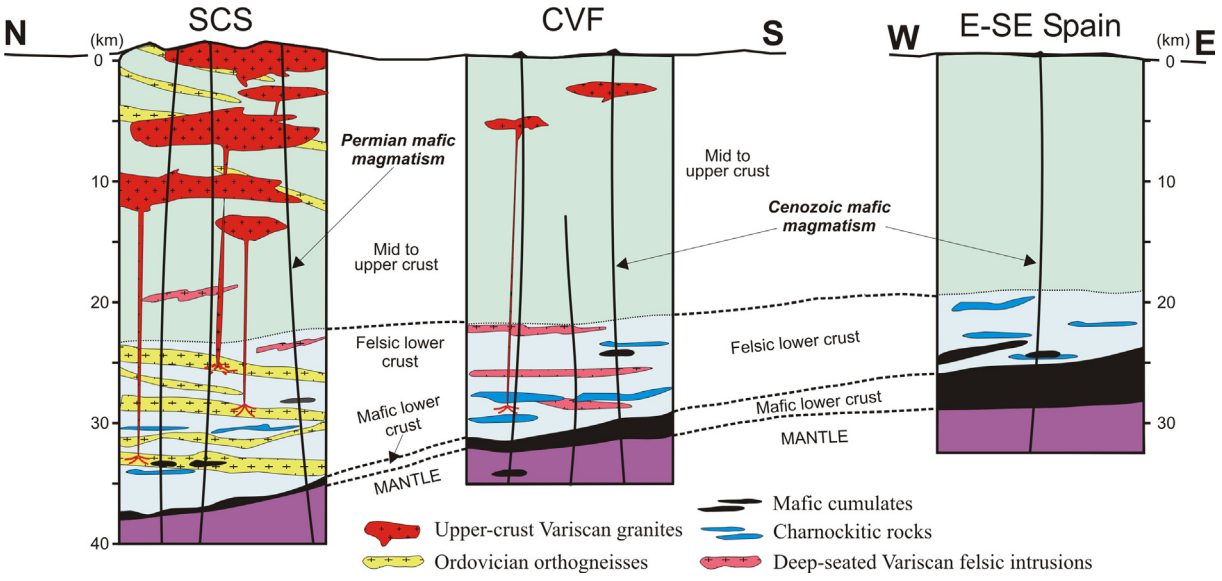

Fig. 14. Schematic crustal sections for the Spanish Central System (left), the Calatrava Volcanic Field (centre) and E–SE volcanic regions from Spain (right) based on the type and abundance of lower crustal xenoliths carried by Permian and Cenozoic mafic igneous rocks (see references in the discussion). Distance between crustal sections is not to scale (see Fig. 1). Moho depth in each section has been taken from Diaz et al. (2021).

11. Conclusions

Our new sampling of granulitic xenoliths from the Calatrava Volcanic Field, together with results from a previous study, supports the presence of three felsic lower crustal xenolith types in this area: charnockitic, metagranitic, and peraluminous metasediments.

Mineral chemistry, whole-rock (major, trace elements and Sr–Nd isotopes) geochemistry and zircon U–Pb geochronology results indicate that the metagranites and charnockitic granulite protoliths represent Variscan magmas (308–313 Ma) stagnated and crystallized in the lower crust and coeval with other magmatic rocks which intruded into shallower crustal levels. Their slightly enriched Sr–Nd isotopic composition suggests that these magmas could be derived from metaigneous and metasedimentary rocks formed in Early Paleozoic or Neoproterozoic times in the context of a subduction environment. Thus, the CVF garnet-bearing felsic granulites display a distribution of U–Pb zircon ages more akin to a Neoproterozoic sedimentary protolith, and their geochemical features point to a non-pelitic original sediment (graywackes–arkoses).

The Calatrava xenoliths represent a felsic lower crust, similarly to what has been observed in the SCS. However, the metaigneous xenoliths from Calatrava are related to Variscan magmas, whereas a phase of older magmatism (Ordovician–Neoproterozoic) is the main constituent of the SCS lower crust.

Both the SCS and Calatrava granulite xenoliths display zircon rims and neoformed grains of metamorphic origin. The temperature and pressure estimations are coherent with HT (for the CVF) and UHT (for the SCS) granulite-facies conditions and anatexis, although more extreme *P-T* values are characteristic of the SCS samples. A mostly coeval interval of 275–299 Ma is proposed for the granulite-facies conditions in both areas. The U–Pb isotopic resetting of zircon at such high temperatures was a long-lasting process maintained during the recovering of the pre-collisional thermal conditions, and might explain the discrepancy between younger granulitization ages and the age of granitic intrusions (~285–316 Ma), interpreted as melts extracted from the lower crust.

The zircon Hf isotopes, along with their geochronological data, indicate that the lower crust under central Spain is mainly composed of metaigneous and metasedimentary rocks associated to the Cadomian continental arc developed in the northern margin of Gondwana, mostly during the Neoproterozoic. These granullite xenoliths provide evidence of mixing between a juvenile and an enriched component, the latter representing the evolution of an Eburnean crust. The most evolved isotopic composition of detrital zircons is likely related to recycling of an older crust (Archean component) derived from North Africa cratonic terranes.

Declaration of Competing Interest

The authors declare that they have no known competing financial interests or personal relationships that could have appeared to influence the work reported in this paper.

Acknowledgements

We acknowledge Alfredo Fernández Larios and Manuel Alpiste for their assistance with the electron microprobe analyses in the CAI of Microscopía Electrónica (UCM) and the LA-ICP-MS analyses in the Instituto Andaluz de Ciencias de la Tierra, respectively. We also thank Pilar Montero for the work carried out during zircon preparation and analysis in the IBERSIMS laboratory (University of Granada). Two anonymous reviewers are acknowledged for their constructive revisions which has helped to improve the initial manuscript. The LA-ICPMS laboratory at the University of Johannesburg was funded by NRF-NEP grant #93208, and is supported by PPM and the CoE DSI-NRF CIMERA; opinions expressed and conclusions arrived at, are those of the author(s) and are not necessarily to be attributed to the CoE. This work is included in the objectives of, and supported by, the PID2020-115980 GB-I00 research project of the Ministerio de Ciencia e Innovación of Spain.

Appendix A. Supplementary data

Supplementary data to this article can be found online at https://doi.org/10.1016/j.gsf.2022.101525.

References

Álvarez-Valero, A., Waters, D.J., 2010. Partially melted crustal xenoliths as a window into sub-volcanic processes: Evidence from the Neogene Magmatic Province of the Betic cordillera, SE Spain. J. Petrol. 51, 973–991.

Amelin, Y., Lee, D.C., Halliday, A.N., 2000. Early–middle Archaean crustal evolution deduced from Lu-Hf and U-Pb isotopic studies of single zircon grains. Geochim. Cosmochim. Acta 64, 4205–4225.

Ancochea, E., 1982. Evolución Espacial y Temporal del Volcanismo Reciente de España Central. Ph.D. thesis, Universidad Complutense de, Madrid, Madri.

Ancochea, E., Huertas, M.J., 2004. La región volcánica del Levante. In: Vera, J.A. (Ed.), Geología De España. Sociedad Geológica de España-Instituto Geológico y Minero de España, Madrid, pp. 675–676.

Ancochea, E., Nixon, P.H., 1987. Xenoliths in the Iberian Peninsula. In: Nixon, P.H. (Ed.), Mantle Xenoliths. Wiley, Chichester, pp. 119–124.

Arenas, R., Martínez Catalán, J.R., Sánchez Martínez, S., Fernández-Suárez, J., Andonaegui, P., Pearce, J.A., Corfu, F., 2007. The Vila de Cruces ophiolite: A remnant of the early Rheic ocean in the variscan suture of Galicia (Northwest Iberian Massif). J. Geol. 115, 129–148.

Avigad, D., Gerdes, A., Morag, N., Bechstädt, T., 2012. Coupled U–Pb–Hf of detritalzircons of Cambrian sandstones from Morocco and Sardinia: Implications for provenance and Precambrian crustal evolution of North Africa. Gondwana Res. 21, 690–703.

Belousova, E.A., Griffin, W.L., ÓReilly, S.Y., Fisher, N.I., 2002. Igneous zircon: trace element composition as an indicator of source rock type. Contrib. Mineral. Petrol. 143, 602–622.

Bianchini, G., Braga, R., Langone, A., 2013. Cristal xenoliths from Tallante (Betic Cordillera, Spain): insights into the crust-mantle boundary. Geol. Mag. 150, 952–958.

Bianchini, G., Braga, R., Langone, A., Natali, C., Tiepolo, M., 2015. Metasedimentary and igneous xenoliths from Tallante (Betic Cordillera, Spain): Inferences on crust-mantle interactions and clues for post-collisional volcanism magma sources. Lithos 220–223, 191–199.

Black, L.P., Kamo, S.L., Allen, C.M., Aleinikoff, J.N., Davis, D.W., Korsch, R.J., Foudoulis, C., 2003. TEMORA 1: a new zircon standard for Phanerozoic U–Pb geochronology. Chem. Geol. 200, 155–170.

Black, L.P., Kamo, S.L., Allen, C.M., Davis, D.W., Aleinikoff, J.N., Valley, J.W., Mundil, R., Campbell, I.H., Korsch, R.J., Williams, I.S., Foudoulis, C., 2004. Improved $^{206}Pb/^{238}U$ microprobe geochronology by the monitoring of a trace-element-related matrix effect; SHRIMP, ID–TIMS, ELA–ICP–MS and oxygen isotope documentation for a series of zircon standards. Chem. Geol. 205, 115–140.

Bouvier, A., Vervoort, J.D., Patchett, P.J., 2008. The Lu-Hf and Sm-Nd isotopic composition of CHUR: Constraints from unequilibrated chondrites and implications for the bulk composition of terrestrial planets. Earth Plane. Sci. Lett. 273, 48–57.

Carracedo, M., Paquette, J.L., Alonso Olazabal, A., Santos Zalduegui, J.F., García de Madinabeitia, S., Tiepolo, M., Gil Ibarguchi, J.I., 2009. U-Pb dating of granodiorite and granite units of the Los Pedroches Batholith. Implications for geodynamic models of the southern Central Iberian Zone (Iberian Massif). Int. J. Earth Sci. 98, 1609–1624.

Cherniak, D.J., Watson, E.B., 2003. Diffusion in zircon. In: Hanchar, J.M., Hoskin, P.W.O. (Eds.), Zircon. Reviews in Mineralogy and Geochemistry 53. Virginia (USA), Mineralogical Society of America, 113–143.

Corfu, F., Hanchar, J.M., Hoskin, P.W.O., Kinny, P., 2003. Atlas of zircon textures. In: Hanchar, J.M., Hoskin, P.W.O. (Eds.), Zircon. Reviews in Mineralogy and Geochemistry 53, Mineralogical Society of America, 469–500.

Diaz, J., Torne, M., Vergés, J., Jiménez-Munt, I., Martí, J., Carbonell, R., Schimmel, M., Geyer, A., Ruiz, M., García-Castellanos, D., Alvarez-Marrón, J., Brown, D., Villaseñor, A., Ayala, C., Palomeras, I., Fernandez, M., Gallart, J., 2021. Four decades of geophysical research on Iberia and adjacent margins. Earth Sci. Rev. 222, 103841.

Donaire, T., Pascual, E., Pin, C., Duthou, J.L., 1999. Two-stage granitoid-forming event from an isotopically homogeneous crustal source: The Los Pedroches batholith, Iberian Massif, Spain. GSA Bullet. 111, 1897–1906.

Downes, H., Dupuy, C., Leyreloup, A.F., 1990. Crustal evolution of the Hercynian belt of western Europe: Evidence from lower-crustal granulitic xenoliths (French Massif Central). Chem. Geol. 83, 209–231.
Ennih, N., Liegeois, J.P., 2008. The boundaries of the West African Craton, with special reference to the basement of the Moroccan Metacratonic Anti-Atlas Belt. Geol. Soc. London Spec. Publ. 297, 1–17.
Errandonea, J., Carracedo Sánchez, M., Sarrionandia, F., Santos Zalduegui, J.F., García de Madinabeitia, S., Gil Ibarguchi, J.I., 2017. The late-Variscan peraluminous Valdepeñas pluton (southern Central Iberian Zone). Geol. Acta 15, 361–378.
Fernández-Suárez, J., Arenas, R., Jeffries, T.E., Whitehouse, M.J., Villaseca, C., 2006. A U-Pb study of zircons from a lower crustal granulite xenolith of the Spanish central system: A record of Iberian lithospheric evolution from the Neoproterozoic to the Triassic. J. Geol. 114, 471–483.
Fernández-Suárez, J., Gutiérrez-Alonso, G., Pastor-Galán, D., Hofmann, M., Murphy, J.B., Linnemann, U., 2014. The Ediacaran–Early Cambrian detrital zircon record of NW Iberia: possible sources and paleogeographic constraints. Int. J. Earth Sci. 103, 1335–1357.
Ferry, J.M., Watson, E.B., 2007. New thermodynamic models and revised calibrations for the Ti-in-zircon and Zr-in-rutile thermometers. Contrib. Mineral. Petrol. 154, 429–437.
García Serrano, J., Villaseca, C., Pérez-Soba, C., 2021. Depleted lherzolite xenoliths from the leucititic Morrón de Villamayor volcano (Calatrava volcanic field, Spain). Lithos 380–381, 105830.
García-Arias, M., Díez-Montes, A., Villaseca, C., Blanco-Quintero, I.F., 2018. The Cambro-Ordovician Ollo de Sapo magmatism in the Iberian Massif and its Variscan evolution: A review. Earth-Sci. Rev. 176, 345–372.
García-Rodríguez, M., Orejana, D., de Ignacio, C., 2022. Petrografía y química mineral de los enclaves de granulitas máficas del volcán de Cofrentes: naturaleza de la corteza inferior bajo la zona este de la Península Ibérica. SS–SS, Geogaceta XX.
González-Jiménez, J.M., Villaseca, C., Griffin, W.L., O'Reilly, S.Y., Belousova, E., Ancochea, E., Pearson, N.J., 2014. Significance of ancient sulfide PGE and Re–Os signatures in the mantle beneath Calatrava, Central Spain. Contrib. Mineral. Petrol. 168, 1047.
Hacker, B.R., Kelemen, P.B., Behn, M.D., 2015. Continental lower crust. Ann. Rev. Earth Planet. Sci. 43, 167–205.
Hoskin, P.W.O., Schaltegger, U., 2003. The composition of zircon and igneous and metamorphic petrogenesis. In: Hanchar, J.M., Hoskin, P.W.O. (Eds.), Zircon. Reviews in Mineralogy and Geochemistry 53. Virginia (USA), Mineralogical Society of America, 27–62.
Heinrich, E.W., Levinson, A.A., Levandowski, D.W., Hewitt, C.H., 1953. Studies in the natural history of micas. University of Michigan, Engineering Research Institute. Ann Arbor. Project M978.
Hoskin, P.W.O., Black, L.P., 2000. Metamorphic zircon formation by solid-state recrystallization of protolith igneous zircon. J. Metam. Geol. 18, 423–439.
Jacobs, J., Opås, B., Elburg, M.A., Läufer, A., Estrada, S., Ksienzyk, A.K., Damaske, D., Hofmann, M., 2017. Cryptic sub-ice geology revealed by a U-Pb zircon study of glacial till in Dronning Maud Land, East Antarctica. Prec. Res. 294, 1–14.
Jiménez-Díaz, A., Ruiz, J., Villaseca, C., Tejero, R., Capote, R., 2012. The thermal state and strength of the lithophere in the Spanish Central System and Tajo Basin from crustal heat production and thermal isostasy. J. Geodyn. 58, 29–37.
Kunz, B.E., Regis, D., Engi, M., 2018. Zircon ages in granulite rocks: decoupling from geochemistry above 850 °C. Contrib. Mineral. Petrol. 173, 26.
Le Maitre, R.W., (Ed.)„ et al., 2002. A Classification of Igneous Rocks and Glossary of Terms: Recommendations of the International Union of Geological Sciences, Subcommission on the Systematics of Igneous Rocks. Cambridge University Press, Cambridge, p. 236.
Li, C.-F., Chen, F., Li, X.-H., 2007. Precise isotopic measurements of sub-nanogram Nd of standard reference material by thermal ionization mass spectrometry using the NdO^+ technique. Int. J. Mass Spec. 266, 34–41.
López-Guijarro, R., Armendáriz, M., Quesada, C., Fernández Suárez, J., Murphy, J.B., Pin, C., Bellido, F., 2008. Ediacaran–Palaeozoic tectonic evolution of the Ossa Morena and Central Iberian zones (SW Iberia) as revealed by Sm–Nd isotope systematics. Tectonophysics 461, 202–214.
Ludwig, K.R., Mundil, R., 2002. Extracting reliable U-Pb ages and errors from complex populations of zircons from Phanerozoic tuffs. Geochim. Cosmochim. Acta 66 (Supp. 1), 463.
McDonough, W.F., Sun, S.S., 1995. The composition of the Earth. Chem. Geol. 120, 223–253.
Merino–Martínez, E., Villaseca, C., Orejana, D., Pérez-Soba, C., Belousova, E., Andersen, T., 2014. Tracing magma sources of three different S-type peraluminous granitoid series by in situ U-Pb geochronology and Hf isotope zircon composition: The Variscan Montes de Toledo batholith (central Spain). Lithos 200–201, 273–298.
Nemchin, A.A., Giannini, L.M., Bodorkos, S., Oliver, N.H.S., 2001. Ostwald ripening as a possible mechanism for zircon overgrowth formation during anatexis: Theoretical constraints, a numerical model, and its application to pelitic migmatites of the Tickalara Metamorphics, northwestern Australia. Geochim. Cosmochim. Acta 65, 2771–2787.
Orejana, D., Villaseca, C., 2008. Heterogeneous metasomatism in cumulate xenoliths from the Spanish Central System: implications on percolative fractional crystallization of lamprophyric melts. In: Coltorti, M., Grégoire, M. (Eds.), Metasomatism in Oceanic and Continental Lithospheric Mantle. Geol. Soc. London Spec. Publ. 293, 101–120.
Orejana, D., Villaseca, C., Paterson, B.A., 2006. Geochemistry of pyroxenitic and hornblenditic xenoliths in alkaline lamprophyres from the Spanish Central System. Lithos 86, 167–196.
Orejana, D., Villaseca, C., Pérez-Soba, C., López-García, J.A., Billström, K., 2009. The Variscan gabbros from the Spanish Central System: A case for crustal recycling in the sub-continental lithospheric mantle? Lithos 110, 262–276.
Orejana, D., Villaseca, C., Armstrong, R.A., Jeffries, T.E., 2011. Geochronology and trace element chemistry of zircon and garnet from granulite xenoliths: Constraints on the tectonothermal evolution of the lower crust under central Spain. Lithos 124, 103–116.
Orejana, D., Villaseca, C., Valverde-Vaquero, P., Belousova, E.A., Armstrong, R.A., 2012. U-Pb geochronology and zircon composition of late Variscan S- and I-type granitoids from the Spanish Central System batholith. Int. J. of Earth Sci. 101, 1789–1815.
Orejana, D., Merino Martínez, E., Villaseca, C., Andersen, T., 2015. Ediacaran-Cambrian paleogeography and geodynamic setting of the Central Iberian Zone: Constraints from coupled U–Pb–Hf isotopes of detrital zircons. Precambrian Res. 261, 234–251.
Orejana, D., Villaseca, C., Kristoffersen, M., 2020. Geochemistry and geochronology of mafic rocks from the Spanish Central System: Constraints on the mantle evolution beneath central Spain. Geosci. Front. 11, 1651–1667.
Otamendi, J.E., De la Rosa, J., Patiño-Douce, A.E., Castro, A., 2002. Rayleigh fractionation of heavy rare earths and yttrium during metamorphic garnet growth. Geology 30, 159–162.
Patiño Douce, A.E., Beard, J.S., 1995. Dehydration-melting of biotite gneiss and quartz amphibolite from 3 to 15 kbar. J. Petrol. 36, 707–738.
Pettijohn, F.J., Potter, P.E., Siever, R., 1972. Sand and Sandstone. Springer-Verlag, New York, p. 618.
Piazolo, S., Belousova, E., La Fontaine, A., Corcoran, C., Cairney, J.M., 2017. Trace element homogeneity from micron- to atomic scale: Implication for the suitability of the zircon GJ-1 as a trace element reference material. Chem. Geol. 456, 10–18.
Puelles, P., Gil Ibarguchi, J.I., García de Madinabeitia, S., Sarrionandia, F., Carracedo Sánchez, M., Fernández Armas, S., 2019. Granulite-facies gneisses and meta-igneous xenoliths fromthe Campo de Calatrava volcanic field (Spain): Implications for the tectonics of the Variscan lower crust. Lithos 342–343, 114–134.
Reche, J., Martínez, F.J., 1996. GPT: An Excel spreadsheet for thermobarometric calculations in metapelitic rocks. Comput. Geosci. 22, 775–784.
Reyes, J., Villaseca, C., Barbero, L., Quejido, A.J., Santos, J.F., 1997. Descripción de un método de separación de Rb, Sr, Sm y Nd en rocas silicatadas para estudios isotópicos. Congreso Ibérico de Geoquímica I 46–55 (in Spanish).
Rubatto, D., Williams, I.S., Buick, I.S., 2001. Zircon and monazite response to prograde metamorphism in the Reynolds Range, central Australia. Contrib. Mineral. Petrol. 140, 458–468.
Rudnick, R.L., Gao, S., 2003. Composition of the continental crust. In: Holland, H.D., Turekian, K.K. (Eds.), Treatise on Geochemistry 3. The crust, Oxford, Elsevier-Pergamon, pp. 1–64.
Scarrow, J.H., Molina, J.F., Bea, F., Montero, P., 2009. Within-plate calc-alkaline rocks: Insights from alkaline mafic magma–peraluminous crustal melt hybrid appinites of the Central Iberian Variscan continental collision. Lithos 110, 50–64.
Schaltegger, U., Fanning, C.M., Guenther, D., Maurin, J.C., Schulmann, K., Gebaurer, D., 1999. Growth, annealing and recrystallization of zircon and preservation of monazite in high-grade metamorphism; Conventional and in-situ U-Pb isotope, cathodoluminiscence and microchemical evidence. Contrib. Mineral. Petrol. 134, 186–201.
Simancas, F., González Lodeiro, F., Expósito, I., Azor, A., Martínez Poyatos, D., 2002. Opposite subduction polarities connected by transform faults in the Iberian Massif and western European Variscides. In: Martínez Catalán, J.R., Hatcher, R. D., Arenas, R., Díaz García, F. (Eds.), Variscan–Appalachian dynamics: the building of the Late Palaeozoic basement. Geol. Soc. Am. Spec. Paper 364, 253–262.
Sisson, T.W., Ratajeski, K., Hankins, W.B., Glazner, A.F., 2005. Voluminous granitic magmas from common basaltic sources. Contrib. Mineral. Petrol. 148, 635–661.
Skjerlie, K.P., Johnston, A.D., 1996. Vapour-absent melting from 10 to 20 kbar of crustal rocks that contain multiple hydrous phases: Implications for anatexis in the deep to very deep continental crust and active continental margins. J. Petrol. 37, 661–691.
Slama, J., Kosler, J., Pedersen, R.B., 2007. Behaviour of zircon in high-grade metamorphic rocks: Evidence from Hf isotopes, trace elements and textural studies. Contrib. Mineral. Petrol. 154, 335–356.
Söderlund, U., Patchett, P.J., Vervoort, J.D., Isachsen, C.E., 2004. The ^{176}Lu decay constant determined by Lu-Hf and U-Pb isotope systematics of Precambrian mafic intrusions. Earth Planet. Sci. Lett. 219, 311–324.
Spear, F.S., 1993. Metamorphic Phase Equilibria and Pressure–Temperature–Time Paths. Mineralogical Society of America, Washington, p. 799.
Springer, W., Seck, H.A., 1997. Partial fusion of basic granulites at 5 to 15 kbar: Implications for the origin of TTG magmas. Contrib. Mineral. Petrol. 127, 30–45.
Sun, S.S., McDonough, W.F., 1989. Chemical and isotopic systematics of oceanic basalts; implications for mantle composition and processes. In: Saunders, A.D., Norrey, M.J. (Eds.), Magmatism in Ocean Basins. Geol. Soc. London Spec. Publ. 42, 313–345.
Talavera, C., Montero, P., Bea, F., González Lodeiro, F., Whitehouse, M., 2013. U–Pb Zircon geochronology of the Cambro–Ordovician metagranites and metavolcanic rocks of central and NW Iberia. Int. J. Earth Sci. 102, 1–23.
Talavera, C., Montero, P., Martínez Poyatos, D., Williams, I.S., 2012. Ediacaran to Lower Ordovician age for rocks ascribed to the Schist–Graywacke Complex

(Iberian Massif, Spain): evidence from detrital zircon SHRIMP U–Pb geochronology. Gondwana Res. 22, 928–942.
Tomkins, H.S., Powell, R., Ellis, D.J., 2007. The pressure dependence of the zirconium-in-rutile thermometer. J. Meta. Geol. 25, 703–713.
Ugidos, J.M., Valladares, M.I., Barba, P., Ellam, R.M., 2003. The Upper Neoproterozoic–Lower Cambrian of the Central Iberian Zone, Spain: Chemical and isotopic (Sm–Nd) evidence that the sedimentary succession records an inverted stratigraphy of its source. Geochim. Cosmochim. Acta 67, 2615–2629.
Ugidos, J.M., Sánchez-Santos, J.M., Barba, P., Valladares, M.J., 2010. Upper Neoproterozoic series in the Central Iberian, Cantabrian and west Asturian Leonese Zones (Spain): Geochemical data and statistical results as evidence for a shared homogenised source area. Precambr. Res. 178, 51–58.
Villaseca, C., Barbero, L., Rogers, G., 1998. Crustal origin of Hercynian peraluminous granitic batholiths of central Spain: Petrological, geochemical and isotopic (Sr, Nd) arguments. Lithos 43, 55–79.
Villaseca, C., Downes, H., Pin, C., Barbero, L., 1999. Nature and composition of the lower continental crust in central Spain and the granulite–granite linkage: inferences from granulitic xenoliths. J. Petrol. 40, 1465–1496.
Villaseca, C., Orejana, D., Pérez-Soba, C., Reyes, J., 2005. Estimación del régimen térmico y producción de calor de los niveles litosféricos del Sistema Central Español. Geogaceta 38, 215–218 (in Spanish).
Villaseca, C., Orejana, D., Paterson, B.A., 2007a. Zr–LREE rich minerals in residual peraluminous granulites, another factor in the origin of low Zr–LREE granitic melts? Lithos 96, 375–386.
Villaseca, C., Orejana, D., Paterson, B., Billström, K., Pérez-Soba, C., 2007b. Metaluminous pyroxene-bearing granulite xenoliths from the lower continental crust in central Spain: Their role in the genesis of Hercynian I-type granites. European J. Mineral. 19, 463–477.
Villaseca, C., Bellido, F., Pérez-Soba, C., Billström, K., 2009. Multiple crustal sources for post-tectonic I-type granites in the Hercynian Iberian Belt. Mineral. Petrol. 96, 197–211.
Villaseca, C., Ancochea, E., Orejana, D., Jeffries, T.E., 2010. Composition and evolution of the lithospheric mantle in central Spain: Inferences from peridotite xenoliths from the Cenozoic Calatrava volcanic field. Geol. Soc. London Spec. Publ. 337, 125–151.
Villaseca, C., Belousova, E.A., Orejana, D., Castiñeiras, P., Pérez-Soba, C., 2011. Presence of Palaeoproterozoic and Archean components in the granulite-facies rocks of central Iberia: The Hf isotopic evidence. Precambr. Res. 187, 143–154.
Villaseca, C., Orejana, D., Belousova, E.A., 2012. Recycled metaigneous crustal sources for S- and I-type Variscan granitoids from the Spanish Central System batholith: Constraints from Hf isotope zircon composition. Lithos 153, 84–93.
Villaseca, C., Merino, E., Oyarzun, R., Orejana, D., Pérez-Soba, C., Chicharro, E., 2014. Contrasting chemical and isotopic signatures from Neoproterozoic metasedimentary rocks in the Central Iberian Zone (Spain) of pre-Variscan Europe: Implications for terrane analysis and Early Ordovician magmatic belts. Precambr. Res. 245, 131–145.
Villaseca, C., Merino Martínez, E., Orejana, D., Andersen, T., Belousova, E., 2016. Zircon Hf signatures from granitic orthogneisses of the Spanish Central System: Significance and sources of the Cambro-Ordovician magmatism in the Iberian Variscan Belt. Gondwana Res. 34, 60–83.
Villaseca, C., García Serrano, J., Orejana, D., 2020. Pyroxenites and megacrysts from alkaline melts of the Calatrava Volcanic Field (central Spain): inferences from trace element geochemistry and Sr–Nd isotope composition. Front. Earth Sci. 8, 132.
Weis, D., Kieffer, B., Maerschalk, C., Barling, J., de Jong, J., Williams, G.A., Hanano, D., Pretorius, W., Matielli, N., Scoates, J.S., Goolaerts, A., Friedman, R.M., Mahoney, J. B., 2006. High-precision isotopic characterization of USGS reference materials by TIMS and MC-ICP-MS. Geochem. Geophys. Geosystems 7. https://doi.org/10.1029/2006GC001283.
Whitehouse, M.J., Platt, J.P., 2003. Dating high-grade metamorphism—constraints from rare-earth elements in zircon and garnet. Contrib. Mineral. Petrol. 145, 61–74.